HHS Public Access

Author manuscript

Cell Stem Cell. Author manuscript; available in PMC 2019 February 01.

Published in final edited form as:

Cell Stem Cell. 2018 February 01; 22(2): 221–234.e8. doi:10.1016/j.stem.2018.01.003.

Adult neurogenesis is sustained by symmetric self-renewal and differentiation

Kirsten Obernier[1,2], **Arantxa Cebrian-Silla**[3], **Matthew Thomson**[4,5,6], **José Ignacio Parraguez**[1,2], **Rio Anderson**[1,2], **Cristina Guinto**[1,2], **José Rodas Rodriguez**[1,2], **José-Manuel Garcia-Verdugo**[3], and **Arturo Alvarez-Buylla**[1,2,7,*]

[1]Eli and Edythe Broad Institute for Stem Cell Research and Regeneration Medicine, University of California, San Francisco, CA 94143, USA

[2]Department of Neurological Surgery, University of California, San Francisco, CA 94143, USA

[3]Laboratory of Comparative Neurobiology, Instituto Cavanilles, Universidad de Valencia, CIBERNED, Valencia, 46980, Spain

[4]Center for Systems and Synthetic Biology, University of California, San Francisco, CA 94158, USA

[5]Department of Cellular and Molecular Pharmacology, University of California, San Francisco, CA 94158, USA

[6]Division of Biology and Biological Engineering, California Institute of Technology Pasadena, CA 91125, USA

Summary

Somatic stem cells have been identified in multiple adult tissues. Whether self-renewal occurs symmetrically or asymmetrically is key to understanding long-term stem cell maintenance and generation of progeny for cell replacement. In the adult mouse brain, neural stem cells (NSCs; B1 cells) are retained in the walls of the lateral ventricles (ventricular-subventricular zone; V-SVZ). The mechanism of B1 cell retention into adulthood for lifelong neurogenesis is unknown. Using multiple clonal labeling techniques we show that the vast majority of B1 cells divide symmetrically. While 20-30% symmetrically self-renew and can remain in the niche for several months before generating neurons, 70-80% undergo consuming divisions generating progeny, resulting in the depletion of B1 cells over time. This cellular mechanism decouples self-renewal

*corresponding author: alvarezbuyllaa@ucsf.edu (A.A.-B.).

[7]Lead contact

Author Contributions

Conceptualization, K.O. and A.A.B; Methodology, K.O., A.C.S., M.T.; Formal Analysis, K.O., A.C.S., M.T.; Investigation, K.O., A.C.S., J.I.P.G., R.A., C.G. and J.R.R; Software, M.T.; Resources, J.M.G.V. and A.A.B.; Writing - Original Draft, K.O., A.C.S., M.T. and A.A.B.; Visualization, K.O., A.C.S., M.T.; Supervision, J.M.G.V., A.A.B.; Funding Acquisition, K.O. and A.A.B..

Declaration of Interests

A.A.-B. is Co-founder and on the Scientific Advisory Board of Neurona Therapeutics.

from the generation of progeny. Limited rounds of symmetric self-renewal and consuming symmetric differentiation divisions can explain the levels of neurogenesis observed throughout life.

eTOC Blurb

Obernier et al. show that juvenile/adult neural stem cells (NSCs) generate progeny or self-renew through symmetric divisions. The prevailing consuming symmetric divisions progressively deplete NSCs, yet this mechanism enables lifelong generation of large numbers of neurons for the olfactory bulb while decoupling proliferation from differentiation.

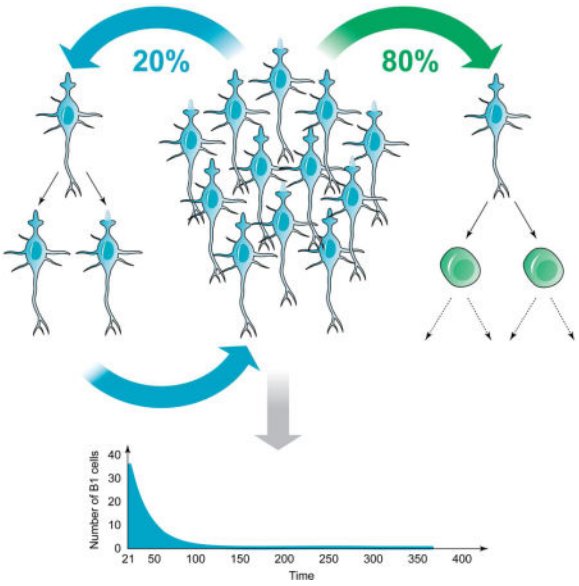

Introduction

Most adult organs retain a population of somatic stem cells for the replacement of differentiated tissue-specific cell types. The brain was considered an exception, until the discovery of adult neurogenesis (Altman, 1962; Goldman and Nottebohm, 1983; Paton et al., 1985) and the isolation and *in vitro* propagation of cells with stem cell properties, i.e. self-renewal and multilineage differentiation (Gage et al., 1995; Kilpatrick and Bartlett, 1993; Reynolds and Weiss, 1992). From this early work it was inferred that the adult brain retains a population of neural stem cells (NSCs) with long-term self-renewal properties. NSCs have been identified in two regions of the adult mammalian brain, the ventricular-subventricular zone (V-SVZ) in the walls of the lateral ventricles and in the subgranular zone (SGZ) next to the dentate gyrus in the hippocampus (for reviews see: (Gage, 2002; Kriegstein and Alvarez-Buylla, 2009; Ming and Song, 2011)). Both regions, which significantly differ in their organization and types of neurons they produce, sustain the generation of young neurons throughout life in mice.

NSCs in the adult V-SVZ are derived from RG during mid-embryonic development (Fuentealba et al., 2015; Merkle et al., 2004). V-SVZ NSCs correspond to a subpopulation

of glial fibrillary acidic protein (GFAP)+ astroglial cells (B1 cells) (Doetsch et al., 1999), which contact the lateral ventricle (LV) and have a long basal process ending on blood vessels (BV) (Mirzadeh et al., 2008; Shen et al., 2008; Tavazoie et al., 2008). After their production in the embryo, V-SVZ NSCs remain mostly quiescent until reactivated during postnatal life (Fuentealba et al., 2015; Furutachi et al., 2015). V-SVZ NSCs generate transient amplifying cells (C cells) that divide three to four times (Ponti et al., 2013) before generating young migrating neurons (neuroblasts, A cells) (Doetsch et al., 1999). These neuroblasts travel from the V-SVZ through the rostral migratory stream (RMS) to the olfactory bulb (OB) (Lois and Alvarez-Buylla, 1994; Lois et al., 1996) where they differentiate into local interneurons (Imayoshi et al., 2008; Lois et al., 1996; Luskin, 1993; Petreanu and Alvarez-Buylla, 2002). The mechanism of NSC retention is key to understanding how neurogenesis is sustained for extended periods of time.

Somatic stem cells can be maintained and generate progeny through asymmetric divisions, or by symmetric self-renewal and symmetric differentiation (Morrison and Kimble, 2006; Shahriyari and Komarova, 2013). Recent data suggest that the majority of NSC in the adult SGZ (Bonaguidi et al., 2011; Encinas et al., 2011) and V-SVZ (Calzolari et al., 2015) undergoes asymmetric cell division - similar to embryonic radial glia (RG) (Noctor et al., 2004), yet direct evidence for the division mode of adult NSCs is missing.

Here we used short-term and long-term lineage tracing methods and show that NSC retention in the adult mouse V-SVZ and sustained production of OB neurons are mainly achieved through symmetric divisions. The majority of NSCs becomes consumed by the symmetric generation of C cells; a smaller fraction of NSCs symmetrically divides to self-renew, a mode of division directly shown by *ex vivo* live imaging. After their self-renewal, NSCs can remain in the V-SVZ for up to 16 weeks (and beyond) before they symmetrically generate C cells and become consumed. Thus, V-SVZ/OB neurogenesis is mainly sustained by population asymmetry of bona fide NSCs.

Results

The majority of B1 cells generate C cells

To investigate whether NSCs touching the LV (B1 cells) self-renew, we stereotaxically injected RCAS retrovirus expressing GFP (RCAS-GFP) into the LV of postnatal (P21-P30) *hGFAP::Tva* mice (Doetsch et al., 1999; Holland and Varmus, 1998) (Fig. 1A; note: one daughter cell will express GFP as RCAS integrates during M-phase). Two to seven days (d2-d7) after injection, we analyzed the entire V-SVZ in whole-mount preparations. On average we found 6 +/− 2.7 clones/whole-mount (5.6 +/− 0.4 mm^2), indicating sparse clonal labeling (Tab. S2 and Fig. S1A-C). We found clones consisting of single GFP+ cells or discrete and tightly packed cell clusters (Fig. 1; neuroblasts that had migrated away were not included in our analysis). The majority of clones contained only C cells (137/171 clones in n= 32 whole-mounts, d2-d7; Fig.1D-F), suggesting that the majority of dividing NSCs had undergone lineage progression. As expected (Ponti et al., 2013), C cells divided about once a day, increasing the size of C cell clusters over the first four days (Fig. 1C). Consistent with the progression of C cells to neuroblasts we observed a rapid accumulation of GFP+ neuroblasts after four days, increasing the total number of GFP+ cells (Fig.1B, F and Fig. S1E).

We also identified clones consisting only of NSCs, indicating self-renewal of B1 cells (33/171 clones; Fig. 2B-C). The majority were single NSCs (secondary NSCs) and five out of 33 NSC-clones consisted of pairs of (tertiary) NSCs (Fig. 2D). Interestingly, four of these pairs were found at later time-points (d4-d7: 4/15 NSC-clones in pairs) and one on d2-d3 (1/18 NSC-clones in pairs). This suggests that within a week a subpopulation of secondary NSCs underwent symmetric self-renewal. We also found one mixed clone containing NSCs and C cells on d5 (1/171 clones; Fig. S1G).

We next estimated the proportion of self-renewing versus C cell generating divisions on d2-d3 before the peak in neuroblast generation. We found 18 GFP+ NSC-clones and 56 GFP+ C cell clusters, accounting for ~25% and ~75% of all divisions, respectively (n=16 mice, Tabs. S1&2). We also injected RCAS at P60 and analyzed whole-mounts on d3 (n=3). We found one secondary GFP+ NSC and 20 clusters containing only GFP+ C cells.

To determine whether self-renewing cells are bona fide NSCs and can divide again to generate progeny or self-renew, we analyzed the V-SVZ two or four weeks after RCAS injection at P21. In addition to 27 secondary NSCs, we found six pairs of tertiary NSCs and one triplet (also see below; Fig. S5C, Tab. S1). This suggests that secondary NSCs, produced at the time of RCAS injection, continued to divide and self-renewed symmetrically for up to a month, generating pairs of tertiary NSCs. We also found 16 clusters of C cells. As C cells rapidly differentiate into neuroblasts that leave the V-SVZ within a few days, clusters found two or four weeks after RCAS injection originated from reactivated secondary or tertiary NSCs. Strikingly, the majority of C cell clusters were devoid of NSCs (~75%, 12/16 clusters; Fig. 2E,F). Four clusters were mixed (Fig. S5B) and could either be derived from asymmetric cell division of secondary NSCs or asynchronous re-activation of pairs of tertiary NSCs.

These data suggest that the majority of dividing NSCs generates C cells and a smaller number self-renews. However, due to RCAS labeling only one daughter cell it is unclear whether clones observed at short survivals resulted from symmetric or asymmetric divisions.

The vast majority of C cells are generated at the expense of NSCs

To label both daughter cells we used sparse Cre/loxP labeling (Bonaguidi et al., 2011). First, to ensure that clusters of C cells were the result of lineage-traced NSCs (and not C cells), we labeled their embryonic predecessor, Nestin+ RG (Fuentealba et al., 2015; Furutachi et al., 2015). Time-mated pregnant *Nestin::Cre^{ERT2};Ai14* or *Nestin::Cre^{ERT2};confetti* (Lagace et al., 2007) females received a single dose of Tamoxifen (Tx) at E17.5 and the V-SVZ of the offspring was analyzed in whole-mounts at P21 or P60 (Figs. 3A-B, S2A-C). At both ages, we observed pairs of NSCs (not shown); however, their origin is unclear as they could be derived from symmetric divisions of RG (Fuentealba et al., 2015; Furutachi et al., 2015) or NSCs postnatally. The majority of clusters of tdTomato (tdT)+ C cells were devoid of NSCs (~60-70%; P21: 8/11; P60: 8/13) (Figs. 3B, S2B, C). Thus, long-term lineage tracing suggests that the vast majority of NSCs divides symmetrically. Asymmetric cell division is rare or does not occur: mixed clusters with longer survivals could be derived from asynchronous reactivation of sister NSCs around the time of analysis.

We next induced sparse expression of the reporter tdT in GFAP+ cells at P21 in *hGFAP::Cre^{ERT2};Ai14* mice (Casper et al., 2007). To further ensure clonal events were derived from dividing progenitors, mice received 5-Bromo-2′-deoxyuridine (BrdU) in the drinking water for three days prior analysis (Fig. 3C). Only samples with less than six tdT +BrdU+ clusters per whole-mount were included in the analysis (Fig. 3D′ & Tab. S3). On d3, we found 15 tdT+BrdU+ clusters of C cells, and none contained NSCs (Tab. S3). Consistent with Cre^{ERT2}-induced recombination labeling both daughter cells, tdT+BrdU+ C cell clusters contained on average ~2-fold more cells than those in our RCAS experiment (Fig. 3D). This suggests that C cells were produced by consuming divisions of NSCs. In a separate experiment we further lowered Tx concentration to obtain labeling of less than one clonal event per hemisphere (Tab. S4). In mice analyzed on d1, d3, or d7, we found 21 C cell clusters, all devoid of NSCs (Fig. S2G-J & Tab. S4; n= 35 hemispheres from 26 mice). The percentage of tdT+BrdU+ C cell clusters over the total number of (quiescent, BrdU-) tdT+ NSCs increased ~three fold from d1-d3 to d7 (Fig. S2K & Tab. S4). The number of C cell clusters/hemisphere does not significantly change during this period (Fig. S2K & Tab. S4), indicating that C cell clusters must arise from recombined NSCs, which continuously undergo activation and consumption.

C cell clusters were also devoid of NSCs when Tx and 3d BrdU were given at P21 to *hGFAP::Cre^{ERT2};confetti* mice (Snippert et al., 2010) (12 C cell clusters; Fig. 3H-J) or to *hGFAP::Cre^{ERT2};Ai14* mice at P60 or P180 (15 C cell clusters and 8 C cell clusters, respectively; Fig. 3E-F). The level of cell death among NSCs was extremely low (~ one cleaved Caspase-3+GFP+ NSC per lateral wall in GFAP::GFP mice; Fig. S2L). It is therefore unlikely that elimination of cells would mask asymmetric cell divisions. Altogether, these data indicate that in the juvenile, adult, and aged V-SVZ, the majority -if not all - of C cells are generated at the expense of NSCs.

NSCs self-renew symmetrically

Whole-mounts of *hGFAP::Cre^{ERT2};Ai14* mice three days after Tx and BrdU administration at P21, P60, or P180 also contained pairs of double-labeled NSCs (three NSC pairs at P21, two at P60, and one pair at P180; Fig. 3K, L, Tab. S3). This indicates that a subpopulation of NSCs (at P21: ~17%) divided symmetrically, possibly a mechanism of self-renewal, and is consistent with pairs of tertiary NSCs in our RCAS experiment above (Fig. 2D). Thus, our data indicate that the majority of GFAP+ NSCs -if not all - divide symmetrically: most are consumed by the generation of C cells and about 1/5 symmetrically self-renews.

Given their complex morphology, how can NSCs divide symmetrically to generate two NSCs? To directly observe the behavior of NSCs within their niche, we performed *ex vivo* time-lapse imaging on organotypic whole-mount cultures from *hGFAP::Cre^{ERT2};Ai14* or *hGFAP::Cre^{ERT2};Ai14;FucciS/G2/M* mice (Sakaue-Sawano et al., 2008) for four days (Fig. 4A and Fig. S3A, D). NSCs frequently extended and retracted lateral processes and occasionally shifted the position of their basal end foot along the vascular surface (Fig. 4D′). Similar to *in vivo* (Fig. S3G, H), we observed that NSCs had cell-cell interactions with neighboring dividing (Fucci+) cells (green arrowheads in Fig. 4C, D″). We recorded 23 dividing tdT+ NSCs, which maintained their basal processes and generated GFAP+Ascl1-

daughter cells that outgrew a new basal process (Fig. 4B,C,E and movies S1&S2). None of these cells divided any further within up to 65h after the initial division. We also recorded lineage progression of C cells (Fig. S3E and data not shown). C cells divided on average every 17.2 +/− 6.7 hours, three-four times before giving rise to A cells, which is consistent with the above *in vivo* data and previous findings (Ponti et al., 2013). Interestingly, initiation of lineages can occur after a lag phase of about two days (Fig. S3E) and the cells on top of the lineages lacked a basal process typical for NSCs. Surprisingly, we observed six NSCs retracting their basal processes; two of these cells divided ~two days later at the end of the imaging period, generating cells that lacked basal processes (Fig. S3F). NSCs primed to generate progeny may lose the basal process before symmetrically generating C cells, while NSCs undergoing symmetric self-renewal maintain the basal process as they divide.

Taken together, *ex vivo* imaging demonstrates that a subpopulation of NSCs divides symmetrically, generating daughter cells that can inherit/grow a basal process. This is consistent with our *in vivo* findings of pairs of NSCs, indicating that a subpopulation of NSCs undergoes symmetric self-renewal.

B1 cells decline in number over time

We hypothesize that the preponderance of consuming divisions reduces the numbers of NSCs over time. We counted the numbers of apical contacts of B1 cells in whole-mounts at different ages (P21, P60, P180 and P360; Fig. 5A, B). The overall density of B1 cells was ~ 4-fold higher at P21 compared to P60 (Fig. 5A, B, D). Similar results were obtained when comparing P60 to P360, consistent with previous reports (Shook et al., 2012). We used the B1 cell numbers obtained experimentally (Fig. 5D) and mathematically modeled their decline from P21 to P60 with symmetric divisions using coupled ordinary differentiation equations (see Methods). The model predicts that in order to attain the decline in B1 cell numbers seen *in vivo*, the probability of consumption (pc) must exceed the probability of symmetric self-renewal (ps) with pc -ps = 0.4. With ps =0.3 and pc =0.7, the level of consuming divisions (~70%) is similar to our short-term lineage tracings (Tab. S1), indicating that dynamics within the B1 cell population can be explained by symmetric divisions.

Interestingly, while B1 cells drastically decline over time, the generation of newborn neurons was less affected by the age of the mouse. Mice received BrdU in their drinking water for one week at different ages (P21, P49, P77, P105, P116, P180, P360) and the densities of newborn neurons in the OB granule cell layer were quantified four weeks later. The number of newborn neurons decreased dramatically over time (Fig. 5C, D). However, this decline did not follow the same dynamics than the decline in B1 cells (Fig. 5D; also see Fig. S4A and Discussion). For example, compared to P21, the density of B1 cells at P180 declined by 95.6 +/− 2.8% whereas the density of BrdU+ granule neurons generated around this age declined by 65.5 +/− 4.7% (Fig. 5D).

We conclude that the preponderance of consuming divisions in the V-SVZ leads to a drastic decline in B1 cells as the organism ages. Neurogenesis also declines with age, but at a slower rate compared to the decline in B1 cells.

Apical B1 cells give rise to non-apical B2 cells

Our data indicate that NSCs can self-renew symmetrically. To investigate whether the daughter cells correspond to B1 cells, we studied the apical surface of GFP+ NSCs three days, two weeks, or four weeks after RCAS injection at P21 (Fig. 6A). On d3, we found 10 GFP+ secondary NSCs with a small apical ending in the center of a pinwheel, indicating self-renewal of B1 cells (Fig. 6B). However, we also found two GFP+ NSCs that had a long basal process contacting blood vessels but lacked contact with the LV. Surprisingly, two and four weeks after virus injection, only half of the GFP+ NSCs with long basal processes contacted the LV (5/8 cells at two weeks and 17/32 cells at four weeks; Fig. 6C-D). Non-apical GFP+ NSCs were sometimes located in the SVZ below the layer of neuroblasts (Fig. 6C′). These cells had astrocytic properties with basal processes and about half were GFAP + (5/11; Fig. S5E). Interestingly, besides pairs of B1 cells, we found pairs of non-apical NSCs (Fig. S5D) and a triplet consisting of one B1 cell and a pair of non-apical NSCs in close proximity (Fig. S5C). Our data suggest that GFP+ B1 cells give rise to non-apical NSCs.

The apical process of B1 cells can be very thin, which could challenge their detection using confocal microscopy. We therefore used electron microscopy (EM) and serial 3D reconstruction to study label-retaining cells (LRCs) four weeks after ^{3}H-thymidine injections at P21 or P60 (Figs. 6E, F & S5F). Ultrastructural analysis confirmed the presence of apical B1 cells (Fig. S5G) and astrocytic non-apical LRCs (Fig. 6I″&I‴) expressing GFAP (Fig. 6N). Non-apical LRCs had lateral and basal processes (Fig. 6G-I) and occasionally contacted BVs (Fig. 6I) and fractones (Kerever et al., 2007) (Fig. 6H). Non-apical LRCs had ultrastructural characteristics similar to previously described B2 cells (Doetsch et al., 1997; Mirzadeh et al., 2008) and importantly, their 9+0 primary cilia were located on the basal side of the cell (away from the LV; Fig. 6G′, M). B2 cells have been shown to proliferate in the adult and aged brain (Capilla-Gonzalez et al., 2014; Doetsch et al., 1997) but their function is unknown (see Discussion). Our data shows that B2 cells are lineage-related to B1 cells.

Self-renewing NSCs can generate progeny after extended periods

We next investigated whether self-renewing NSCs are bona fide stem cells and contribute interneurons to the OB later in life. We administered BrdU in the drinking water to *hGFAP::Tva* mice four weeks after RCAS injection at P21. The OBs were analyzed after an additional four weeks to allow neurons to migrate into the OB and differentiate (Fig.7A). We found GFP+BrdU+ neurons (NeuN+) in the OB (Fig. 7C), indicating that a subpopulation of NSCs self-renewed at P21 (GFP-label) and generated neurons four weeks later (BrdU-label) (Fig. 7B and Tabs. S5 & S6). In addition, GFP+ neuroblasts were present in the RMS and V-SVZ (Fig. 7D, E and not shown), indicating that some GFP+ NSCs generated progeny after BrdU administration. Furthermore, when we extended the interval between RCAS injection and BrdU administration to eight or twelve weeks, at both time-points GFP+BrdU+ interneurons were found in the granule cell layer and periglomerular layer, and GFP+ migrating neuroblasts in the RMS (Fig. 7F, G). These data indicate that NSCs that had self-renewed at P21 generated neurons three to four months later.

The reactivation to produce progeny was not unique to NSCs that had self-renewed at juvenile stages (P21) but also occurred later in life. We injected RCAS into *hGFAP::Tva* mice at P60 and administered BrdU four weeks later (Fig. 7A). After an additional four weeks, we found GFP+BrdU+ neurons in the OB (Fig. 7C). Thus, self-renewing adult NSCs also became re-activated and generated neurons (although at lower rates than self-renewing NSCs in the juvenile V-SVZ; Fig. 7C).

To confirm the above observations, RCAS was injected at P21 into *hGFAP::Tva;hGFAP::Cre^{ERT2};Ai14* mice followed by Tx administration four weeks later (Fig. S6A). After four additional weeks, we found GFP+tdT+ labeled neurons in the OB (Fig. S6B, C). To label larger cohorts of dividing cells, we administered BrdU for one week to *hGFAP::Cre^{ERT2};Ai14* mice at P21 and then induced recombination (Tx) in GFAP+ cells at different times: simultaneously with BrdU administration, immediately after the end of BrdU administration, or two, four, eight, 12 or 16 weeks after BrdU. Four weeks after Tx administration, the OB was analyzed for BrdU+tdT+ neurons (Fig. 7H-J). As expected, the density of BrdU+tdT+ neurons was highest in the group that received BrdU and Tx simultaneously, but then decreased (Fig. 7I, Fig. S6E). This observation is in line with our findings above, suggesting that the majority of NSCs undergoes consuming divisions; only a relatively small fraction self-renews and generates neurons later (at or after the time of Tx administration). The density of double-labeled neurons then remained constant, suggesting similar reactivation of BrdU label-retaining NSCs, before it declined.

Taken together, these data indicate that GFAP+ NSCs can generate young neurons up to four-five months after their self-renewing division. This indicates that V-SVZ NSCs, through a preponderance of symmetric cell division, sustain a pool of primary progenitors for the generation of OB interneurons well into adult life.

Discussion

Control over the pool of somatic stem cells and production of progeny can be achieved by 1) population asymmetry, where symmetric divisions of separate primary progenitors achieve self-renewal and differentiation, or 2) asymmetric cell division, where individual stem cells produce both, a new primary progenitor and differentiated progeny (Hormoz 2013). The mode(s) of division of somatic stem cells is key to understanding how tissues can regenerate throughout life. The largest pool of adult stem cells in the central nervous system is retained in the V-SVZ in the walls of the lateral ventricle. Here we show that most - if not all - GFAP + NSCs in the juvenile (P21) and adult (P60, P180) mouse V-SVZ divide symmetrically. Whereas the majority becomes consumed by the generation of progeny, a fraction maintains the NSC pool by symmetric self-renewal. This is in contrast to the behavior of RG in the embryo, which have been shown to predominantly undergo asymmetric self-renewal (Miyata et al., 2001; Noctor et al., 2004). Our data suggest that in the adult V-SVZ asymmetric cell divisions are rare or do not occur. Instead, symmetrically self-renewing NSCs can remain in the V-SVZ for several months before they generate progeny.

The majority of V-SVZ NSCs becomes consumed generating progeny

Our short-term lineage tracing (d2-d7) shows that the majority of NSCs, independent of the age of the mouse, divide symmetrically to generate progeny. It is unlikely that asymmetric cell divisions are masked by cell death, as the numbers of cleaved Caspase-3+ NSCs was very low. It could be possible that the TVA receptor (RCAS) or Cre may be transmitted to early C cells, resulting in labeling of secondary progenitors. However, the majority of C cell clusters were devoid of NSCs upon long-term lineage tracing of RG during embryonic development or of postnatal NSCs. The small number of mixed clusters observed (Tab. S1) could be due to a rare population of NSCs undergoing asymmetric cell division. However, as mixed clusters were mostly observed at longer survivals, it is more likely that they resulted from asynchronous re-activation of secondary NSCs; the symmetric consumption of one NSC within a pair would result in a C cell cluster next to the sister NSC, which did not divide. Consistently, embryonic retroviral barcoding for lineage tracing has previously shown that the majority of clones of OB interneurons born at or after P28 are not clonally related to interneurons born before P28 (Fuentealba et al., 2015). It is also unlikely that asymmetric cell divisions were masked by retroviral inactivation as the RCAS data were confirmed using Cre^{ERT2} lineage tracing. Moreover, dual hits (of neighboring cells or the same cell) during RCAS transduction must be rare; the majority of GFP+ cells at early time-points after RCAS injection were single cells. Moreover, as clusters of C cells form, they did not contain NSCs and were about half the size of clusters labeled in our Cre^{ERT2}/BrdU experiment; a strong indication that both labeling methods were clonal.

V-SVZ NSCs self-renew symmetrically

Our *in vivo* data show that ~20% of NSCs undergo symmetric self-renewal and generate two secondary NSCs, which either enter quiescence or become sporadically reactivated. Previous studies have revealed the presence of LRCs in the V-SVZ (Doetsch et al., 1999), which are generally assumed to correspond to NSCs (Furutachi et al., 2015). We show that LRCs are bona fide stem cells that self-renew before generating progeny, which can occur immediately or with a lag of up to four to five months, and possibly beyond. Until they generate neurons, secondary NSCs self-renew symmetrically or remain quiescent. Extended periods of quiescence have also been shown for the precursors of NSCs, which are generated from RG during mid-fetal development and become reactivated in postnatal life (Fuentealba et al., 2015; Furutachi et al., 2015). In the postnatal and adult V-SVZ, the majority of reactivated cells become consumed generating progeny. Interestingly, a subpopulation can symmetrically self-renew for at least one to two additional rounds. A recent report in the hematopoietic system revealed that throughout life, adult label-retaining hematopoietic stem cells asynchronously undergo four rounds of symmetric amplification (Bernitz et al., 2016). It will be interesting to determine whether there is a limit to the number of times V-SVZ NSCs can self-renew symmetrically. We also do not know whether newly generated NSCs after symmetric divisions, although competent to generate neurons weeks or months after their generation, are exactly equivalent to the mother NSC.

In contrast to our data, it has recently been proposed that V-SVZ NSCs undergo rapid rounds of asymmetric cell divisions within three to five weeks before becoming consumed (Calzolari et al., 2015). This study used *Glast::*Cre^{ERT} mice crossed with the confetti

reporter and over time observed a progressive increase in the sizes of OB clones. However, it is unknown whether multiple generation of OB neurons are due to asymmetric NSC divisions or symmetric NSC self-renewal and sporadic reactivation of the sister cells. It is also possible that detection of three confetti colors is not sufficient for clonal analysis in the OB. Putative clones containing both, deep and superficial granule neurons (Calzolari et al., 2015) are in sharp contrast to the regional specification that exists in the V-SVZ (Merkle et al., 2007). Retroviral barcode lineage tracing has shown that deep and superficial granule neurons are derived from distinct progenitors specified very early in embryonic development (Fuentealba et al., 2015). Nevertheless, it is possible that multiple adult NSC populations co-exist. Although GLAST and GFAP (current study) are largely co-expressed by NSCs (Beckervordersandforth et al., 2010; Codega et al., 2014; Platel et al., 2009), we cannot exclude that the different Cre-drivers label different NSC populations or that V-SVZ NSCs may modify their mode of division under certain conditions, as it has been suggested for hippocampal NSCs (Bonaguidi et al., 2012; DeCarolis et al., 2013). However, while hippocampal NSCs share astrocytic properties with V-SVZ NSCs, they are not found next to the LV but form a displaced germinal matrix next to the dentate gyrus where they generate excitatory granule neurons. In contrast to what we describe here for the V-SVZ, long-term lineage tracings suggest that the majority of hippocampal NSCs divide asymmetrically (Bonaguidi et al., 2011; Encinas et al., 2011). Interestingly, a small fraction of hippocampal NSCs were found in pairs, suggesting some level of symmetric self-renewal (Bonaguidi et al., 2011) although it remains unknown whether these cells can function as long-term progenitors of new neurons. In contrast, by following the clones derived from V-SVZ NSCs within the first few days of labeling we find little evidence for asymmetric self-renewal, while a small number of mixed clusters appeared with longer survivals.

That V-SVZ NSCs, despite their complex morphology, self-renew symmetrically was also confirmed by time-lapse imaging of V-SVZ explants. The majority of self-renewing NSCs maintained their basal process as they underwent cytokinesis, similar to RG (Noctor et al., 2004). The period of time we were able to keep the V-SVZ *ex vivo* (four days) did not allow us to observe the initiation of C cell lineages from NSCs. The C cell lineages we observed *ex vivo* were possibly initiated from NSCs at an earlier time-point *in vivo*, prior to dissection. Our time-lapse recordings were performed on V-SVZ explants from P21-P35 mice as tissue from older mice (P60) showed decreased cell viability after about one day in culture. We cannot exclude that the mode(s) of division would change depending on age. However, in vivo lineage tracings using Cre^{ERT2} combined with BrdU at different ages (P21, P60, and P180) revealed similar findings. Activated NSCs *in vivo* up-regulate Nestin and Ascl1 (Codega et al., 2014; Pastrana et al., 2009) (Fig. S2A). However, none of the recorded NSCs expressed Ascl1::GFP (in *hGFAP::Cre^{ERT2};Ai14;Ascl1::GFP* mice; not shown) or were Ascl1+ in post-imaging immunostaining (Fig. 4E). It is possible that factors in the CSF (Lehtinen et al., 2011; Zappaterra et al., 2007) and/or factors from the vasculature (Kokovay et al., 2010; Ramírez-Castillejo et al., 2006; Shen et al., 2004) as well as the CSF flow (Sawamoto et al., 2006) are not present in our *ex vivo* preparations but essential for lineage initiation. Single cell sequencing recently suggested that activated NSCs could be subdivided into self-renewing NSCs and NSCs primed for differentiation. These distinct molecular states are associated with the loss of astrocytic genes and mediators of self-renewal and

acquisition of pro-neural genes (Dulken et al., 2017). Interestingly, a small subpopulation of NSCs retracted their basal process during imaging, which may indicate early conversion into C cells. We also found evidences of retraction of the basal process *in vivo* (Fig. S5C′). NSCs that lose their basal process may be primed to generate progeny later. This process retraction may be part of the activation process and together with the formation of lineages of C cells may take more than four days, requiring longer imaging periods. *In vivo* live imaging may help clarify the cellular dynamics associated with lineage progression and reveal whether rare asymmetric divisions occur.

Symmetric stem cell divisions have been observed in other tissues, e.g. during early development in C. elegans germ cells (Kimble and White, 1981), the adult mouse epidermis (Rompolas et al., 2016), mammalian embryonic and adult hematopoietic stem cells (Bernitz et al., 2016; Kimble and White, 1981; Morrison et al., 1995), the intestinal epithelium(Snippert et al., 2010), and as a mechanism for the amplification and tangential expansion of early chicken neuroepithelial cells (Gray and Sanes, 1992). In contrast to symmetric divisions, were self-renewal and differentiation are decoupled, asymmetric divisions result in fixed ratios of differentiation and self-renewal, incapable of replenishing the stem cell pool upon injury. The number of divisions required to maintain the stem cell pool for extended periods is lower using population asymmetry compared to asymmetric cell division, possibly lowering replicative aging and somatic mutations (Hormoz, 2013; Shahriyari and Komarova, 2013). Symmetrically self-renewing divisions in the V-SVZ may offer dynamic control over the numbers of NSCs, as it has been suggested for other tissues (Morrison and Kimble, 2006).

B1 cells generate B2 cells

While the above show that V-SVZ NSCs self-renew symmetrically, we do not know whether secondary NSCs are exactly equivalent to the mother NSC. Interestingly, our study revealed that a subpopulation of self-renewing B1 cells loses the apical contact and generates non-apical B2 cells. The lack of specific markers to label and lineage trace B2 cells currently hampers experimental approaches to determine B2 cell function. A subpopulation of B2 LRCs cells had dark cytoplasm under EM (not shown), indicating high densities of free ribosomes recently associated with the transition from quiescent to activated NSCs (Dulken et al., 2017; Llorens-Bobadilla et al., 2015). Our data indicate that while the number of B1 cells sharply declines with age, the decline in neurogenesis is less pronounced. This could be explained by age-related changes in proliferation of C or A cells resulting in larger clones, or decrease in cell death. However, while the discrepancy in levels of neurogenesis and B1 cell number is already pronounced by P60, cell death of OB neurons in the GCL is similar from P10 to P60 (Fiske and Brunjes, 2001). We also found no difference in clone size three days after RCAS injection at P21 or P60 (3.1 +/− 1.6 versus 3.4 +/− 0.2 GFP+ cells/C cell cluster, respectively; and data not shown), suggesting that cell cycle length of C cells may not be affected by the age of the mouse. Another possible explanation is that B2 cells serve as a reserve population of NSCs as B1 cells are depleted.

If we assume that B2 cells are a reservoir of adult NSCs and use differential equations to predict how these cells would behave to maintain the levels of neurogenesis observed *in vivo*

(assuming constant cell death and clonal size), we can derive the following predictions: 1) B2 would peak in size at approximately P50 (Fig. S4B upper graph); 2) B2 cells would need to have approximately equal probabilities of symmetric self-renewal and consumption; and 3) B2 cells undergo one to two rounds of self-renewing divisions before becoming consumed (also see Methods). This is consistent with the pairs of B2 cells observed in our long-term RCAS experiments. Similar to non-apical label-retaining B2 cells, the recently identified outer RG also lose apical contact with the ventricle (Florio and Huttner, 2014; Hansen et al., 2010). Outer RG have been mainly described in the development of large brains, likely as a mechanism to expand populations of neurons. Our quantification and modeling estimates that over the life of a mouse, the V-SVZ produces approximately ten million neurons. This is more than twice the total number of neurons in the mouse cerebral cortex. B2 cells could be key to explain the very large numbers of new OB neurons produced in the V-SVZ throughout life. Testing this hypothesis will require methods to specifically lineage-trace B2 cells.

The progenitor dynamics shown here - with the vast majority of NSCs undergoing symmetric cell divisions - could support neurogenesis with a minimum number of self-renewing divisions, which may protect the primary progenitor population from accumulating genetic defects. Unlike asymmetric stem cell self-renewal, the mechanism we propose here results in a gradual depletion of NSCs. This process seems to be carefully choreographed to propel neurogenesis, albeit at progressively lower levels, for the life span of a mouse. It is possible that similar mechanisms may limit neurogenesis to infancy in animals that, like humans, have very long life spans (Paredes et al., 2016; Sanai et al., 2011; Wang et al., 2011).

STAR Methods

Contact for Reagent and Resource Sharing

Further information and requests for resources and reagents should be directed to and will be fulfilled by the Lead Contact, Arturo Alvarez-Buylla (alvarezbuyllaa@ucsf.edu)

Experimental Model and Subject Details

Mice—Mice were housed on a 12h day-night cycle with free access to water and food in a specific pathogen-free facility in social cages (up to 5 mice/cage) and treated according to the guidelines from the University of California, San Francisco, Institutional Animal Care and Use Committee (IACUC) and NIH. All mice used in this study were healthy and immuno-competent, and did not undergo previous procedures unrelated to the experiment. Approximately equal numbers of male and female mice were used per experiment.

The following mouse lines of the indicated genotypes were used: *hGFAP::Tva*$^{+}$ mice *(Tg(GFAP-TVA)5Hev/J)* (Holland and Varmus, 1998); *hGFAP::Cre*$^{ERT2+}$ mice *(B6(C3)-Tg(GFAP-cre/ERT2)13Kdmc/Mmmh)*, MMRC (016992-MU) (Casper et al., 2007); *FucciS/G2/M*$^{+}$ mice *(B6.Cg-Tg(FucciS/G2/M)#504Bsi)* RIKEN BRC (RBC02706) (Sakaue-Sawano et al., 2008); *Ascl1::GFP*$^{+}$ mice *(Tg(Ascl1-EGFP)AU176Gsat)* (Gong et al., 2003); *Nestin::Cre*$^{ERT2+}$ mice were obtained by crossing *B6.Cg-Tg(Nes-cre/*

ERT2)Keisc(Lagace et al., 2007) with CD-1 WT mice; *Ai14*$^{+/+}$ *or Ai14*$^{+/-}$ mice *(B6.Cg-Gt(ROSA)26Sortm14(CAG-tdTomato)Hze/J)*, The Jackson Laboratory (007914) (Madisen et al., 2010); *hGFAP::GFP (FVB/N-Tg(GFAPGFP)14Mes/J*, The Jackson Laboratory (003257) (Zhuo et al., 1997); *Confetti*$^{+/WT}$ mice (Gt(ROSA)26Sortm1(CAG-Brainbow2.1)Cle/J, The Jackson Laboratory (013731) (Snippert et al., 2010).

Method Details

Tissue Handling

V-SVZ Whole-mount Dissections: For whole-mount dissections mice were anesthetized with 2.5% Avertin (i.p.) and sacrificed by cervical dislocation. Brains were extracted and the walls of the LV dissected out from the caudal aspect of the telencephalon, hippocampus, and septum (Mirzadeh et al., 2008). After overnight fixation in 4% PFA, whole-mounts were processed for immunohistochemistry.

Perfusion and sectioning: Mice were anesthetized with 2.5% Avertin (i.p.) and transcardially perfused first with saline and then 4% PFA. Brains were removed and fixed overnight in 4% PFA at 4°C. After cryoprotection in 30% sucrose, fixed tissue was cut on a sliding microtome (Leica SM 2010R) into 50 μm coronal sections and processed as floating sections for immunohistochemistry.

Immunohistochemistry: Whole-mounts were incubated in primary and secondary antibodies in PBS with 2% TX-100 and 10% normal goat serum for 48h at 4°C. For s amples processed for BrdU unmasking, incubations with primary and secondary antibodies were performed first, followed by fixation in 4% PFA at room temperature for 10 minutes. Tissue was then incubated in 2N HCl at 37°C for 40 minutes, followe d by treatment with 0.1M boric acid for 20 minutes at RT prior incubation with anti-BrdU antibodies and corresponding secondary antibodies for 48h at 4°C each (Ponti et al., 2013). Coronal sections were processed according the same protocols but with shorter antibody incubation times (primary antibodies: overnight at 4°C; secondary an tibodies: 90 minutes at room temperature). Primary antibodies used were rabbit anti-dsRed (Clontech), chicken anti-GFAP (Abcam), rabbit anti-GFAP (DAKO), mouse anti-GFAP (Millipore), mouse anti-Ascl1 (BD Biosciences), chicken anti-GFP (Aves Lab), guinea pig anti-Doublecortin (Millipore), rabbit anti-BrdU (Abcam), mouse anti-NeuN (Millipore), rabbit anti-gamma-Tubulin (Sigma-Aldrich), mouse anti-beta-Catenin (BD Biosciences), rabbit anti-Ki67 (Novocastra), rat anti-VCAM-1 (BD Pharmingen), rabbit anti-cleaved Caspase-3 (Cell Signaling). Secondary antibodies were conjugated to AlexaFluor dyes (Invitrogen/Molecular Probes). Confocal z-stack images were taken on a Leica SP5 or SP8 white light laser scanning confocal microscope.

Identification of labeled V-SVZ cells—The identity of GFP or tdT labeled cells was determined based on marker expression (NSCs: GFAP+; C cells: Ascl1+; neuroblasts: DCX +) and/or morphology. NSCs were identified by their long basal process. C cells were morphologically identified by their bigger, more globular cell body compared to NSCs, and absence of a basal process. Cells with a small cell body and a leading edge were classified as neuroblasts. We refer to C cell clones as isolated events of labeled cells that contain one

(RCAS) or more C cells. Neuroblasts are highly migratory (Wichterle et al., 1997) and we only included those that were tightly associated with labeled clusters in our clonal analysis; neuroblasts that had moved away from clusters were not included as their clonal relationship to cells in clusters is unknown. We define a symmetric division as a division that gives rise to daughter cells of the same cell fate analyzed by morphology and/or marker expression (Noctor et al., 2004). As retroviral labeling only results in labeling of one of the two daughter cells, in our RCAS experiments we refer to single GFP+ NSCs as secondary NSCs (daughter cells), indicating self-renewal. A summary of labeled events can be found in Tabs. S2-S4.

Tamoxifen and BrdU Administration—Tamoxifen (Tx) was prepared at 20 mg/ml in corn oil and administered via oral gavage. BrdU was dissolved in water at 1 mg/ml and administered in the drinking water.

Recombination in Embryonic Radial Glia: Three month-old, timed-pregnant *Nestin::Cre^{ERT2};Ai14* or *Nestin::Cre^{ERT2};confetti* females received a single dose of Tx (1.67-16.7 mg/Kg BW) via oral gavage at embryonic day 17.5 (E17.5). The morning of the plug was considered E0.5.

Recombination and BrdU-labeling of V-SVZ NSCs: Juvenile P21-P30, adult P60, or aged P180 *hGFAP::Cre^{ERT2};Ai14* mice received a single dose of Tx (6.66 mg/Kg BW) and BrdU was administered in the drinking water (1 mg/ml) for three days; whole-mounts of the V-SVZ were prepared at the end of the BrdU treatment. In a separate experiment we further lowered Tx concentration (1.67- 3.33 mg/Kg BW) administered at P21 and mice were sacrificed after one, three, or seven days of BrdU treatment. One day after labeling, most tdT + cells were ependymal cells and NSCs, and we never observed tdT+BrdU+ ependymal cells (Spassky et al., 2005). On average, one whole-mount contained less than one tdT+BrdU+ C cell cluster (Fig. S2K & Tab. S4). We also found single isolated tdT+BrdU+ NSCs at all time-points (~7% of all tdT+ NSCs; Tabs. S3+S4 and data not shown). These cells likely correspond to the growth fraction of NSCs (Ponti et al., 2013).

Lineage Tracing of OB interneurons: P21 *hGFAP::Cre^{ERT2};Ai14* mice received BrdU (1 mg/ml) in the drinking water for one week followed by one dose of Tx (166.7 mg/Kg BW) per day for five consecutive days at different time-points (0-16 weeks after BrdU; see experimental outline Fig. 7H). Mice were sacrificed four weeks after the last Tx administration, perfused, and sections of the OBs were analyzed of BrdU+tdT+ labeled NeuN+ neurons. As a control, brains of mice that did not receive Tx administration were analyzed. The levels of recombination in the absence of Tx was ~180-fold lower than upon Tx injection: while the OB of mice that had received Tx four weeks prior analysis contained 1452 +/− 204 tdT+ cells/mm^2, the age-matched control group without Tx only contained 8 +/− 3 tdT+ cells/mm^2. Moreover, the density of double-labeled cells with a 16 weeks interval was still 4.4-fold higher than in control mice without Tx.

BrdU Birth-dating of OB Interneurons: *hGFAP::GFP* mice or *hGFAP::Cre^{ERT2};Ai14* mice received BrdU in their drinking water for one week at various ages (P21, P49, P77, P105, P116, P180, P360) and the granule cell layer (GCL) of the OB was analyzed in

coronal sections for BrdU+ neurons after four weeks. The densities we described here for newborn neurons generated over time are likely not affected by changes in the volume of the GCL as this has been shown to remain relatively constant over the period of one year (Petreanu and Alvarez-Buylla, 2002).

RCAS Retrovirus—Replication-incompetent avian RCAS-GFP retrovirus was prepared using chicken embryonic fibroblasts DF-1 cells (ATCC) as packaging cells. Cells were grown in DMEM with 10% FBS, 1% Penicillin/Streptomycin at 37°C an d 5% CO2. 6-well culture dishes with 80% confluency of DF-1 cells were transfected with 1 μg of RCAS-GFP plasmid DNA (Chen et al., 1999) using FuGene (Roche). Supernatant was harvested after at least three passages with increasing culture volume, centrifuged for 15 minutes at 13Krpm, and filtered through a 0.45 um filter. Viral solution was then centrifuged in a Beckman ultracentrifuge at 50,000 g at 4°C for 90 m inutes. Viral pellets were resuspended in PBS, aliquoted, and stored at −80°C. Viral titer was determined using serial 2-fold dilutions of the viral stock with quantification of GFP+ labeled DF-1 cells by FACS.

Retroviral Labeling of V-SVZ NSCs: Postnatal (P21-P30) or adult (P60-P120) *hGFAP::Tva* mice were stereotaxically injected with 1 μl RCAS-GFP retrovirus (1.7×10^8 viral particles/ml) unilaterally into the LV using the following coordinates relative to bregma: 0.2 anterior, 0.8 lateral, 2.25 ventral. For clonal analysis, animals were sacrificed at the time-points indicated in the text and whole-mounts were prepared for immunohistochemical analysis.

Retroviral Lineage Tracing of OB Interneurons: Four, eight, or 12 weeks after intraventricular RCAS delivery *hGFAP::Tva* mice received BrdU in their drinking water for one week (1 mg/ml). Alternatively, *hGFAP::Tva;hGFAP::Cre^{ERT2};Ai14* mice received one dose of Tx (166.7 mg/Kg BW) per day for five consecutive days four weeks after viral labeling. Mice were perfused four weeks after the last labeling and forebrains were cut into coronal sections and processed for immunohistochemistry.

Organotypic whole-mount-sliver preparation—For thin sliver preparations of whole-mounts from P21-P35 old *hGFAP::Cre^{ERT2};Ai14*, or *hGFAP::Cre^{ERT2};Ai14;Fucci-S/G2/M*, or *hGFAP::Cre^{ERT2};Ai14;Ascl1::GFP* mice (not shown), brains were dissected in 37°C Leibovitz med ium. After revealing the en-face view of the lateral wall, thin slivers containing the V-SVZ were dissected with a micro stab knife away from the underlying striatum and transferred onto hydrophilic PTFE cell culture inserts (Millipore) with the apical surface of the V-SVZ facing down. Inserts were either placed into 6-well plates (culture experiments) or 6-well plates with custom-made glass imaging windows (MatTek Corporation) (time-lapse imaging). Plates contained custom-made phenol-red free medium with 25% Hanks BSS, 5% FBS, 1% N-2 supplement, 1% Pen/Strep, 1% L-Glutamine, and 2% Glucose (Hansen et al., 2010). To assess *ex vivo* effects on proliferation, explants were kept in 37°C incubators under hypoxic conditions (8% O2) or normoxic conditions and were fixed and stained for Ki67. Whereas both conditions resulted in a decrease of proliferating cells at DIV4, culturing under hypoxic conditions maintained higher levels of Ki67+ cells than normoxic conditions (Fig. S3A′). Explants from adult (P60) mice showed reduced

tissue viability within one day of culturing, therefore *ex vivo* cultures were performed with explants from postnatal (P21-P35) mice.

Time-lapse microscopy—Postnatal (P21-P35) *hGFAP::Cre^{ERT2};Ai14*, or *hGFAP::Cre^{ERT2};Ai14;Fucci-S/G2/M* or *hGFAP::Cre^{ERT2};Ai14;Ascl1::GFP* mice (not shown) received one injection of Tx (6.66-16.66 mg/KG BW) to induce recombination of the Ai14 locus in GFAP expressing cells (note: in contrast to our sparse clonal labeling paradigm, the direct observation of cells allowed a much higher density of tdT+ cells to increase the probability to observe dividing NSCs). Fucci-S/G2/M allowed visualization of nuclei of cells in S, G2, or M phase as azami-green+. Two days after Tx administration, explants were prepared as thin slivers of whole-mount preparations and cultured under hypoxic conditions in imaging plates for at least 2 hours to allow tissue to equilibrate. Plates were transferred into a Ludin chamber (37°C, hypoxic O2 concentrations 5%) mounted onto an inverted Leica SP5 or SP8 white-light laser confocal scanning microscope. To minimize phototoxicity and photobleaching minimal laser power, optimum excitations and detection with high sensitivity HyD detectors, and high-speed scanning (700Hz for SP5; 8000Hz for SP8 equipped with resonant scanner) were used. Z-stack Images were taken every 20-35 minutes over a time period of 3-4 days. Every 8-12h z positions were readjusted to compensate for tissue movements and allow data storage. Under these conditions, we observed very rare events of tdT+ cells undergoing cell death. Consistent with our assessment of proliferation (Ki67+) under culture conditions, live-imaging of postnatal explants from Fucci-S/G1/M mice showed constant levels of proliferation (density of Fucci+ cells/field/time-point) for four days (see Fig. S3D). During imaging, tdT+ NSCs were identified by the presence of their characteristic basal processes. In some experiments, mice received i.v. injections of fluorophore (DyLight 488)-conjugated tomato Lectin (from Lycopersicon esculentum) prior whole-mount dissection to label blood vessels, allowing us to study the interaction of NSCs basal process with the vasculature. C cells were identified by morphology (absence of the basal process, larger globular cell body, non-migratory behavior). For some experiment, the identity of C cells was confirmed using *Ascl1::GFP* mice (data not shown). At the end of the recording period, explants were processed for immunohistochemistry. Imaging files from individual acquisitions we compiled and analyzed using Imaris Image Analysis software (v7.6-8.2, Bitplane).

Electron microscopy and Autoradiography—Postnatal P21 or adult P60 *hGFAP::GFP* mice received two i.p. injections of ^{3}H-thymidine (1.67 µl/g body weight, specific activity 5Ci/mmol; Perkin Elmer, USA) 12h apart for seven days (n= 4 and 3 mice, respectively). Mice were perfused with 2% PFA-2.5% glutaraldehyde four weeks after the last injection. Brains were removed, postfixed in the same fixative overnight, rinsed in 0.1 M PB, and cut into 200 µm sections using the vibratome. Sections were postfixed in 2% osmium, dehydrated, and embedded in Araldite (Durcupan, Fluka). Semithin sections (1.5 µm) were cut with a diamond knife. Subsequently, V-SVZ semithin sections were dipped in autoradiography emulsion (Carestream Autoradiography Emulsion, Type NTB), dried in the dark, and stored at 4°C for four weeks (Doetsch et al., 1997). Autoradiography was developed using standard methods and counterstained with 1% toluidine blue. ^{3}H-Thymidine labeled nuclei in the V-SVZ were identified in semithin sections. In order to

consider a cell labeled, five or more autoradiography grains needed to be present over the nucleus. The nucleus also had to be labeled in at least three consecutive serial sections. Consecutive sections showing labeled cells were selected under a light microscope (Nikon, Eclipse), re-embedded, and ultrathin-sectioned (70nm) for TEM analysis (Tecnai Spirit G2, FEI, Oregon).

Immunogold staining: For GFAP pre-embedding immunogold staining, mice were perfused with 4% PFA-0.5% glutaraldehyde, in PB 0.1M. Brains were removed and post-fixed with 4% PFA overnight. 50 μm floating sections were incubated with antibodies against GFAP (1:250, Dako, Z0334) for 72h at 4°C. 0.8 nm colloidal gold ultrasmall secondary antibodies were used and the size of gold particles were increased with the Silver Enhancement kit (Aurion, EMS). Sections were contrasted with 1% osmium and embedded in Durcupan. Semithin sections were prepared, selected at the light microscope level and cut into 70 nm ultrathin sections.

Mathematical modeling—We incorporated data and inferred lineage relationships to develop a simple mathematical model of the population dynamics of the B1, B2, C, and A cells. The model consists of a set of coupled ordinary differentiation equations. Model parameters (including cell division frequency for B1 and C cells) were determined through experimental measurements when possible (see below and (Ponti et al., 2013)). Equations were solved analytically and simulated using NDsolve in mathematica (Wolfram Mathematica). Differentiation and self-renewal propensities of the B1 and B2 cell populations were determined by numerical minimization of model error calculated as normalized discrepancy between model simulation and experimental data at indicated time-points.

B1 model: We constructed a model to study the impact of measured differentiation/self-renewal rates on the B1 population size and rates of neurogenesis. Our model accounts for the modes of division observed experimentally (symmetric self-renewal and consumption). We take n to be the probability of a B1 cell entering a division cycle in a 24 h period, and we assign each class of division modes observed experimentally a probability (ps symmetric self-renewal; pc consumption). By modeling the stoichiometry of each division mode, we can generate population level rates for each class of event where k1 and k2 are the rates of symmetric self-renewal and symmetric consumption of B1 cells, respectively, and

$$\mathrm{ki} = \mathrm{p\_\ i\ n/tau}$$

so that the rates have a unit of time^{-1}. tau in the duration of a cell division is in units of hours (here 17 h based on (Ponti et al., 2013)).

In this first order model, B1 cells are converted directly into C0 cells (first generation of C cells) through consuming divisions. These C0 cells then undergo a series of additional divisions before generating neuroblasts, that in turn divide once or twice; each lineage branch generates ~16-32 neuroblasts (Ponti et al., 2013). We also fix the rate of C cell divisions, k4.

dB1/dt = − (k1 + k2) B1 + 2 k1 B1,

dC0/dt = 2 k2 B1 − k4 C0,

dC1/dt = 2 k4 C0 − k4 C1,

dC2/dt = 2 k4 C1 − k4 C2,

dC3/dt = 2 k4 C2 − k4 C3,

dA/dt = 2 k4 C3

Parameter values:

n = 0.06;

tau = 17.5/24;

pc = 0.7

ps = 1 − pc;

k2 = n*(pc)/tau;

k1 = n*(ps)/tau;

k4 = 0.95; (Rate of C cell divisions)

In this model, B1 cell population dynamics have a simple analytical solution. We have:

$$\mathrm{dB1/dt} = -(\mathrm{k1}+\mathrm{k2})\mathrm{B1}(\mathrm{t}) + (2\mathrm{k1})\,\mathrm{B1}(\mathrm{t})\,\mathrm{dt} = (\mathrm{k1}-\mathrm{k2})\,\mathrm{B1}(\mathrm{t})$$

This linear differential equation can be solved for B1(t):

$$\mathrm{B1}(\mathrm{t}) = \mathrm{B1}(0)\exp(\mathrm{t}(\mathrm{k1}-\mathrm{k2})) = \mathrm{B1}(0)\exp(\mathrm{t\,n/tau}(\mathrm{ps}-\mathrm{pc}))$$

$$log[\mathrm{B1}(\mathrm{t})/\mathrm{B1}(0) = \mathrm{t\,n/tau}\ (\mathrm{ps}-\mathrm{pc}). \quad \text{(Equation 1)}$$

Quantitatively, based on measurements, we fix tau= 17.5 hours and n = 0.06. In the model, the decay rate of the B1 cell population depends only upon ps-pc (see Equation 1), the difference between the probability of B1 self-renewal and the probability of consuming division. By fitting the experimental data to an exponential decay we can therefore bound this difference. Note that the asymmetric division probability drops out of this expression, as asymmetric events do not change the net size of the cell population.

The fit to experimental data bounds pc-ps = 0.4. We now use the additional experimental measurements that the asymmetric division probability is 0. With this data, we can also set pc+ps = 1. Thus, we find ps = 0.3 (symmetric self-renewal) and pc = 0.7 (consumption). These values are in close agreement with measured probabilities of consumption and self-renewal *in vivo*.

The model predicts a high rate of B1 cell consumption, and similarly the experimental data indicates a rapid decay in B1 population size. Using the above expressions, we can estimate the time scale for B1 population exhaustion as the day when the population size falls below one cell as ~P300. Statistical analysis of this model shows 70% of cells differentiate without undergoing a self-renewing division leading to rapid population decline.

In the B1 base model, neurogenesis rates are directly proportional to B1 population size (amplification factor of 32 (generation of neuroblasts/lineage)), so that in this model neurogenesis and B1 population size experience proportional declines. However, this is inconsistent with the difference observed experimentally between the decline in neurogenesis and the numbers of B1 cells from P21 to P100 (Fig. 6D).

B2 model: We defined a simple extension of the B1 model to incorporate B2 cells as a second population of primary progenitors. We introduce B2 cells into the model as being generated from B1 cells, which is consistent with our analysis of apical B1 and non-apical B2 GFP+ secondary cells (RCAS; Figs. 6A-D and S5B). In the model, B1 cells generate a B2 cell as well as a B1 cell. We then introduce parameters for B2 cell self-renewal rate (psb2) and differentiation rate (pcb2). We fit these parameters to the neurogenesis data while keeping all other parameters fixed and found psb2 = .034 and prb2 = .038, predicting equal rates of self-renewal and differentiation in the model.

$$dB1/dt = -(k1 + k2)\, B1 + k1\, B1,$$

$$dB2/dt = 2\, psb2\, B2 + k1\, B1 - pcb2\, B2 - psb2\, B2,$$

$$dC0/dt = 2\, k2\, B1 - k4\, C0 + 2\, pcb2\, B2,$$

$$dC1/dt = 2\, k4\, C0 - k4\, C1,$$

$$dC2/dt = 2\, k4\, C1 - k4\, C2,$$

$$dC3/dt = 2\, k4\, C2 - k4\, C3,$$

$$dA/dt = 2\, k4\, C3$$

B2 cell Parameters:

psb2 = .034;

pcb2 = .0378;

With these parameters B2 cells experience equal probabilities of differentiation and self-renewal and on average undergo one to two rounds of self-renewal prior to differentiation (50% undergo a single round and 25% two rounds). The process of B1 and B2 cell differentiation are a single step escape processes and so have an exponential waiting time distribution. The implications of this distribution are that there will be a wide range of division and differentiation statistics experiences by cells. For example, if 6% of cells divide each day, then cells on average divide every 16 days. However, the exponential statistics imply that 10% of cells will wait 30 days to divide. With nearly equal probability of self-renewal and differentiation, many B2 cells will undergo more than one cycle of division prior to differentiation so that the average time to differentiation is 35 days. Further, given

similar rates of consumption and self-renewal for B2 cells, the population undergoes a slow decay as a function of time, following the initial burst of B2 cell production from B1 cells.

Note: In numerical simulations of the B1 and B2 models, initial conditions for the model are set to generate 27000 B1 cells at P21, to be consistent with measured B1 cell population size at this time point.

Division frequency of NSCs: To estimate the division frequency of NSCs, we calculated the ratios of tdT+BrdU+ events (clones +B pairs) to tdT+ (BrdU negative) NSCs in our Cre^{ERT}-mediated lineage tracing. In *hGFAP::Cre^{ERT2};Ai14* mice this ratio was 0.058 +/− 0.026 and 0.067 +/− 0.018 at P21 and P60, respectively, indicating that at both ages ~6-7% of labeled NSCs had generated progeny. This is similar to a 8.6% growth fraction recently estimated on a population level at P60. As the mathematical model requires a division frequency of B1 cells of ≥ 4%, we used n= 0.06 in our modeling described above.

Quantification and Statistical Analysis

Quantifications throughout the manuscript are represented as mean +/− SD (standard deviation). Statistical significance was defined as * $p \leq 0.05$, ** $p < 0.01$, *** $p < 0.001$, **** $p < 0.0001$. One-way ANOVA with Tukey's multiple comparisons (Prism GraphPad software) was used to determine statistical significance of multiple comparisons; student's t-test (Excel) was used for pair-wise comparisons between two groups.

Clonal analysis in V-SVZ Whole-mounts—To quantify the numbers of clonal events in the V-SVZ after RCAS retroviral labeling or Cre recombination, a) tile-scans encompassing the entire whole-mount were acquired using a Leica SP8 white light laser scanning confocal microscope and clonal events were manually counted using Imaris Image Analysis software (v7.6-7.8, Bitplane), or b) clonal events were counted live under a Leica SP5 or SP8 white light laser scanning confocal microscope. For RCAS injections, the V-SVZ ipsi-lateral to the injection side was quantified. In rare cases, the contra-lateral hemisphere contained GFP+ events and was included in the analysis (indicated with 'c' in Tab. S2; 4/32 whole-mounts from n=28 mice at all time-points). As the labeling efficiency with RCAS was greater than in Tx/BrdU treated mice and virus injection could potentially result in more focal labeling, we analyzed clonality of GFP+ labeled cells by distance measurement. For this, using a Leica SP8 white light laser scanning confocal microscope we acquired tile-scans of z-stacks encompassing the entire V-SVZ whole-mount on d2-d3 after RCAS injection (n=11 mice). The surface area of whole-mounts (5.6 +/− 0.4 mm^2) was measured and GFP+ C cell clusters and NSCs were mapped using Neurolucida software (MBF Bioscience) (Fig. S1B). Tracings were used for distance measurements between GFP+ events and their nearest GFP+ (using Neurolucida Explorer, MBF Bioscience). The distribution of measured distances between neighboring labeled events is shown in Fig. S1A, with an average distance of 465 μm between events. All of the brains used in the Tx/BrdU labeling experiments had five or less double-labeled cell pairs or clusters per whole-mount. Quantifications of clonal events per time-point/experiment in the Result sections are reported as mean +/− SD. Data in Fig. 1 B (cells/whole-mount) are represented as mean +/− SD.

For quantification of cluster sizes (cells/cluster) confocal images from each clonal event were taken and analyzed in a 3D-view using Imaris Image Analysis software (v7.6-7.8, Bitplane). GFP+ clusters grew in size during the first five days and then decreased, represented in and Fig. 1C as mean +/− SD with p= 0.0413 d2 vs. d4 *; p < 0.0001 d2 vs. d5 ****; p= 0.054 d3 vs. d5 *; p= 0.0116 d5 vs. d7 *. Fig. S1D shows the size of individual clusters and its mean; statistical significance was determined using one-way ANOVA with Tukey's multiple comparisons. The comparison of cluster size between tdT+BrdU+ and GFP+ (RCAS) events on d3 is shown in Fig. 3D and represented as mean +/− SD with p= 0.005; statistical significance was determined applying two-tailed student's t-test with equal variance. N represents the number of mice with n= 6, 9, 3, 3, 3, and 4 *hGFAP::Tva* mice for analysis on d2, d3, d4, d5, d6, and d7 after RCAS injection, respectively (Tab. S2), and n=8 *hGFAP::Cre^{ERT2};Ai14* mice on d3 after Tx/BrdU administration (Tab S3). In a separate set of experiment we used n= 3, 9, and 14 *hGFAP::Cre^{ERT2};Ai14* mice on d1, d3, and d7 after Tx/BrdU administration, respectively (Tab. S4); n= 8 *hGFAP::Cre^{ERT2};confetti* mice were used for Tx and 3d BrdU administration at P21.

For embryonic lineage tracing n=5 and 3 *Nestin::Cre^{ERT2};Ai14* mice were analyzed at P21 or P60, respectively; n= 3 *Nestin::Cre^{ERT2};confetti* mice were analyzed at P21.

Double-labeled OB Interneurons—For analysis of total number of double-labeled RCAS-GFP+BrdU+ interneurons upon RCAS and BrdU sequential labeling with 4 weeks interval, tile-scans of serial sections of the OBs were acquired using a Leica SP8 white light laser scanning confocal microscope. GFP+ and BrdU+ interneurons (expressing NeuN) were counted in 3D using Imaris Image Analysis software (v7.6-7.8, Bitplane) (manual counts of cytoplasmatic RCAS; automated counts of nuclear BrdU+ and co-expression of both labels). Quantifications were blindly confirmed with manual counting using a fluorescence microscope (Olympus AX70, Olympus). Data in the Result section and in Tabs. S5&6 are expressed as mean +/− SD from n=6 *hGFAP::Tva* mice.

For analysis of the percentages or densities of double-labeled interneurons per OB upon sequential labeling with RCAS and BrdU or tdT, or BrdU and tdT, images were acquired with a Leica SP5 or SP8 white light laser scanning confocal microscope. Per experiment, labeled cells were counted in 3-4 images of 5-6 sections per OB/mouse either manually (cytoplasmatic tdT or RCAS) or automated (nuclear BrdU+ and co-expression of cytoplasmatic RCAS or tdT) in 3D with Imaris Image Analysis software (v7.6-7.8, Bitplane). Quantifications were confirmed by an independent experimenter as well as by manual counts on a fluorescent microscope (Olympus AX70) as an alternative approach. Data in Figs. 7C, G, I and S6C, E are represented as mean +/−SD. Statistical significance of the percentage of GFP+BrdU+/GFP+ neurons (Fig. 7C; p= 0.021*) was determined using two-tailed student's t-test with equal variance. Statistical significances of the densities of BrdU+tdT+ neurons with a four week interval vs. eight, 12, or 16 weeks in Fig. 7I (4wk vs. 8wk, p= 0.22, n.s.; 4wk vs. 12 wk, p= 0.022*; 4wk vs 16 wk, p= 0.05 *) and the percentages of BrdU+tdT+/BrdU+ neurons in Fig. S6E (4wk vs. 8wk, p= 0.04 *; 4wk vs. 12 wk, p= 0.0004 ***; 4wk vs 16 wk, p= 0.004 **) were determined using one-tailed student's t-test with equal variance. Sizes of experimental groups using sequential RCAS and BrdU or Tx labeling are: RCAS injection at P21 with four, eight, or 12 weeks chase before BrdU

administration, n= 6, 3 and 3 mice, respectively; RCAS injection at P60 with four weeks chase before BrdU administration, n=3 mice; RCAS injection at P21 followed by Tx four weeks later, n=3 mice. Sizes of experimental groups using sequential BrdU and Tx labeling are: BrdU only (no Tx; control), n= 4 mice; simultaneous administration of BrdU/Tx, n=4 mice; administration of Tx directly after BrdU; n=3 mice; Tx administration two, four, eight, 12, or 16 weeks after BrdU administration, n=4, 3, 5, 3 and 2 mice, respectively.

Birth dating of Interneurons—Upon BrdU administration at different ages, 3-4 images of 5-6 sections per OB were acquired with a Leica SP8 white light laser scanning confocal microscope. BrdU+ neurons were counted in 3D automated using Imaris Image Analysis software (v7.6-7.8, Bitplane). Data were expressed as densities (BrdU+ cells/mm^2 GCL) and are represented in Fig. 5D as mean +/− SD with n= 7, 4, 3, 3, 9, 4, and 3 mice for groups with BrdU administration at P21, P49, P77, P105, P116, P180, or P360, respectively. Compared to P21, the densities of newborn neurons born at P77-P360 declined, with statistical significance determined using one-tailed student's t-test with equal variance (P21 vs P49, p= 0.24, n.s.; P21 vs. P77, p= 0.02 *; P21 vs. P105, p= 0.0015 **; P21 vs. P116, P180, or P360, p ≤ 0.0001 ***).

Apical Surface Analysis—For quantifications of apical surfaces of B1 cells across different ages, V-SVZ whole-mounts from P21, P60, P180 or P360 *hGFAP::GFP* mice (n= 3, 6, 7, and 3 mice respectively) were immunostained for GFP, beta-Catenin and gamma-Tubulin (Mirzadeh et al., 2008). Images (3-4 fields/region; 63x objective) of the apical surface of the anterior-ventral, anterior-dorsal, posterior-dorsal, and posterior-ventral region of lateral walls were acquired with Leica SP5 or SP8 white light laser scanning confocal microscope (Leica). The apical endings of B1 cells were manually counted using beta-Catenin to demarcate of the cell membrane and gamma-Tubulin to indicate basal bodies with Imaris Image Analysis software (v7.6-7.8, Bitplane). Data in Figs. 5D and S4A,B are expressed as density of B1 cells/mm^2 surface area at different time-points normalized to P21 and represented as mean +/− SD.

For identifications of apical B1 and non-apical B2 cells labeled by RCAS-GFP, V-SVZ whole-mounts from *hGFAP::tva* mice were immunostained for GFP, beta-Catenin and gamma-Tubulin or GFAP or VCAM-1 three, 14, or 28 days after injection with RCAS-GFP at P21 (n= 5, 3, and 7 mice, respectively). Images of GFP+ cells were acquired with a Leica SP5 or SP8 white light laser scanning confocal microscope and analyzed in 3D with Imaris Image Analysis software (v7.6-7.8, Bitplane).

Cell Death—V-SVZ whole-mounts of n= 3 P60 hGFAP::GFP mice were stained for cleaved Capsase-3, Ascl1, GFP and DAPI. Per whole-mount 4-5 images were taken using a Leica SP8 white light laser scanning confocal microscope and cleaved Capase-3+ cells were counted in 3D with Imaris Image Analysis software (v7.6-7.8, Bitplane). On average, whole-mounts contained 73 +/− 27 cleaved Caspsae-3+ cells and 1.4 +/− 2.5 GFAP::GFP+/cleaved Caspsae-3+ B cells (mean +/− SD).

Proliferating Cells ex vivo—Ki67+ cells in V-SVZ whole-mount preparations fixed immediately after dissection (dropfix) or after one, four, and five days in organotypic

cultures under hypoxic or five days under normoxic conditions were counted automated using Imaris Image Analysis software (v7.6-7.8, Bitplane) in 3-4 images/sample taken with Leica SP5 or SP8 white light laser scanning confocal microscopes from n= 4, 3, 5, 4, and 3 mice, respectively. Data in Fig. S3A are normalized to the densities of Ki67+ in dropfix samples and represented as mean +/− SD; statistical significance of densities of Ki67+ cells in dropfix vs. DIVs was determined using two-tailed student's t-test with equal variance (p= 0.013*). Fucci+ cells were quantified at consecutive time-points of the same field over the course of up to four days of time-lapse imaging automated using Imaris Image Analysis software (v7.6-7.8, Bitplane). Data in Fig. S3D are represented as mean +/− SD from n= 20 fields from n= 12 whole-mounts.

Supplementary Material

Refer to Web version on PubMed Central for supplementary material.

Acknowledgments

We would like to thank Daniel Lim, Luis Fuentealba, and members of the Alvarez-Buylla lab for helpful discussions. K.O. was supported by the Deutsche Forschungsgemeinschaft (German Research Foundation). A.C.S. and J.M.G.V. were supported by Generalitat Valenciana (PROMETEOII/2014/075). M.T. received support from the NIH Office of the Director (OD), the National Cancer Institute, and the National Institute of Dental & Craniofacial Research (NIDCR) NIH DP5 OD012194 as well as support from the UCSF Center for Systems and Synthetic Biology P50 GM081879. J.I.P.G. was supported by the Chilean Government (Becas Chile). Work in the Alvarez-Buylla laboratory was supported by NIH grants NS028478 & HD032116 and a generous gift from the John G. Bowes Research Fund. A.A.-B. is the Heather and Melanie Muss Endowed Chair and Professor of Neurological Surgery at UCSF.

References

Altman J. Are New Neurons Formed in the Brains of Adult Mammals? Science. 1962; 135:1127–1128. [PubMed: 13860748]

Beckervordersandforth R, Tripathi P, Ninkovic J, Bayam E, Lepier A, Stempfhuber B, Kirchhoff F, Hirrlinger J, Haslinger A, Lie DC, et al. In vivo fate mapping and expression analysis reveals molecular hallmarks of prospectively isolated adult neural stem cells. Cell Stem Cell. 2010; 7:744–758. [PubMed: 21112568]

Bernitz JM, Kim HS, MacArthur B, Sieburg H, Moore K. Hematopoietic Stem Cells Count and Remember Self-Renewal Divisions. Cell. 2016; 167:1296–1309.e10. [PubMed: 27839867]

Bonaguidi MA, Wheeler MA, Shapiro JS, Stadel RP, Sun GJ, Ming GL, Song H. In vivo clonal analysis reveals self-renewing and multipotent adult neural stem cell characteristics. Cell. 2011; 145:1142–1155. [PubMed: 21664664]

Bonaguidi MA, Song J, Ming GL, Song H. A unifying hypothesis on mammalian neural stem cell properties in the adult hippocampus. Curr Opin Neurobiol. 2012; 22:754–761. [PubMed: 22503352]

Calzolari F, Michel J, Baumgart EV, Theis F, Götz M, Ninkovic J. Fast clonal expansion and limited neural stem cell self-renewal in the adult subependymal zone. Nat Neurosci. 2015; 18:490–492. [PubMed: 25730673]

Capilla-Gonzalez V, Cebrian-Silla A, Guerrero-Cazares H, Garcia-Verdugo JM, Quiñones-Hinojosa A. Age-related changes in astrocytic and ependymal cells of the subventricular zone. Glia. 2014; 62:790–803. [PubMed: 24677590]

Casper KB, Kristin J, McCarthy KD. Characterization of astrocyte-specific conditional knockouts. Genesis. 2007; 45:292–299. [PubMed: 17457931]

Chen CM, Smith DM, Peters MA, Samson ME, Zitz J, Tabin CJ, Cepko CL. Production and design of more effective avian replication-incompetent retroviral vectors. Dev Biol. 1999; 214:370–384. [PubMed: 10525341]

Codega P, Silva-Vargas V, Paul A, Maldonado-Soto AR, Deleo AM, Pastrana E, Doetsch F. Prospective identification and purification of quiescent adult neural stem cells from their in vivo niche. Neuron. 2014; 82:545–559. [PubMed: 24811379]

DeCarolis NA, Mechanic M, Petrik D, Carlton A, Ables JL, Malhotra S, Bachoo R, Götz M, Lagace DC, Eisch AJ. In vivo contribution of nestin- and GLAST-lineage cells to adult hippocampal neurogenesis. Hippocampus. 2013; 23:708–719. [PubMed: 23554226]

Doetsch F, García-Verdugo JM, Alvarez-Buylla A. Cellular composition and three-dimensional organization of the subventricular germinal zone in the adult mammalian brain. J Neurosci. 1997; 17:5046–5061. [PubMed: 9185542]

Doetsch F, Caillé I, Lim DA, García-Verdugo JM, Alvarez-Buylla A. Subventricular zone astrocytes are neural stem cells in the adult mammalian brain. Cell. 1999; 97:703–716. [PubMed: 10380923]

Dulken BW, Leeman DS, Boutet SC, Hebestreit K, Brunet A. Single-Cell Transcriptomic Analysis Defines Heterogeneity and Transcriptional Dynamics in the Adult Neural Stem Cell Lineage. Cell Rep. 2017; 18:777–790. [PubMed: 28099854]

Encinas JM, Michurina TV, Peunova N, Park JH, Tordo J, Peterson DA, Fishell G, Koulakov A, Enikolopov G. Division-coupled astrocytic differentiation and age-related depletion of neural stem cells in the adult hippocampus. Cell Stem Cell. 2011; 8:566–579. [PubMed: 21549330]

Fiske BK, Brunjes PC. Cell death in the developing and sensory-deprived rat olfactory bulb. J Comp Neurol. 2001; 431:311–319. [PubMed: 11170007]

Florio M, Huttner WB. Neural progenitors, neurogenesis and the evolution of the neocortex. Development. 2014; 141:2182–2194. [PubMed: 24866113]

Fuentealba LC, Rompani SB, Parraguez JI, Obernier K, Romero R, Cepko CL, Alvarez-Buylla A. Embryonic Origin of Postnatal Neural Stem Cells. Cell. 2015; 161:1644–1655. [PubMed: 26091041]

Furutachi S, Miya H, Watanabe T, Kawai H, Yamasaki N, Harada Y, Imayoshi I, Nelson M, Nakayama KI, Hirabayashi Y, et al. Slowly dividing neural progenitors are an embryonic origin of adult neural stem cells. Nat Neurosci. 2015; 18:657–665. [PubMed: 25821910]

Gage FH. Neurogenesis in the adult brain. J Neurosci. 2002; 22:612–613. [PubMed: 11826087]

Gage FH, Ray J, Fisher LJ. Isolation, characterization, and use of stem cells from the CNS. Annu Rev Neurosci. 1995; 18:159–192. [PubMed: 7605059]

Goldman SA, Nottebohm F. Neuronal production, migration, and differentiation in a vocal control nucleus of the adult female canary brain. Proc Natl Acad Sci U S A. 1983; 80:2390–2394. [PubMed: 6572982]

Gong S, Zheng C, Doughty ML, Losos K, Didkovsky N, Schambra UB, Nowak NJ, Joyner A, Leblanc G, Hatten ME, et al. A gene expression atlas of the central nervous system based on bacterial artificial chromosomes. Nature. 2003; 425:917–925. [PubMed: 14586460]

Gray GE, Sanes JR. Lineage of radial glia in the chicken optic tectum. Development. 1992; 114:271–283. [PubMed: 1576964]

Hansen DV, Lui JH, Parker PRL, Kriegstein AR. Neurogenic radial glia in the outer subventricular zone of human neocortex. Nature. 2010; 464:554–561. [PubMed: 20154730]

Holland EC, Varmus HE. Basic fibroblast growth factor induces cell migration and proliferation after glia-specific gene transfer in mice. Proc Natl Acad Sci U S A. 1998; 95:1218–1223. [PubMed: 9448312]

Hormoz S. Stem cell population asymmetry can reduce rate of replicative aging. J Theor Biol. 2013; 331:19–27. [PubMed: 23623948]

Imayoshi I, Itaru I, Masayuki S, Toshiyuki O, Keizo T, Tsuyoshi M, Masahiro Y, Kensaku M, Toshio I, Shigeyoshi I, et al. Roles of continuous neurogenesis in the structural and functional integrity of the adult forebrain. Nat Neurosci. 2008; 11:1153–1161. [PubMed: 18758458]

Kerever A, Schnack J, Vellinga D, Ichikawa N, Moon C, Arikawa-Hirasawa E, Efird JT, Mercier F. Novel extracellular matrix structures in the neural stem cell niche capture the neurogenic factor fibroblast growth factor 2 from the extracellular milieu. Stem Cells. 2007; 25:2146–2157. [PubMed: 17569787]

Kilpatrick TJ, Bartlett PF. Cloning and growth of multipotential neural precursors: Requirements for proliferation and differentiation. Neuron. 1993; 10:255–265. [PubMed: 8439411]

Kimble JE, White JG. On the control of germ cell development in Caenorhabditis elegans. Dev Biol. 1981; 81:208–219. [PubMed: 7202837]

Kokovay E, Goderie S, Wang Y, Lotz S, Lin G, Sun Y, Roysam B, Shen Q, Temple S. Adult SVZ lineage cells home to and leave the vascular niche via differential responses to SDF1/CXCR4 signaling. Cell Stem Cell. 2010; 7:163–173. [PubMed: 20682445]

Kriegstein A, Alvarez-Buylla A. The glial nature of embryonic and adult neural stem cells. Annu Rev Neurosci. 2009; 32:149–184. [PubMed: 19555289]

Lagace DC, Whitman MC, Noonan MA, Ables JL, DeCarolis NA, Arguello AA, Donovan MH, Fischer SJ, Farnbauch LA, Beech RD, et al. Dynamic contribution of nestin-expressing stem cells to adult neurogenesis. J Neurosci. 2007; 27:12623–12629. [PubMed: 18003841]

Lehtinen MK, Zappaterra MW, Chen X, Yang YJ, Hill AD, Lun M, Maynard T, Gonzalez D, Kim S, Ye P, et al. The cerebrospinal fluid provides a proliferative niche for neural progenitor cells. Neuron. 2011; 69:893–905. [PubMed: 21382550]

Llorens-Bobadilla E, Zhao S, Baser A, Saiz-Castro G, Zwadlo K, Martin-Villalba A. Single-Cell Transcriptomics Reveals a Population of Dormant Neural Stem Cells that Become Activated upon Brain Injury. Cell Stem Cell. 2015; 17:329–340. [PubMed: 26235341]

Lois C, Alvarez-Buylla A. Long-distance neuronal migration in the adult mammalian brain. Science. 1994; 264:1145–1148. [PubMed: 8178174]

Lois C, García-Verdugo JM, Alvarez-Buylla A. Chain migration of neuronal precursors. Science. 1996; 271:978–981. [PubMed: 8584933]

Luskin MB. Restricted proliferation and migration of postnatally generated neurons derived from the forebrain subventricular zone. Neuron. 1993; 11:173–189. [PubMed: 8338665]

Madisen L, Zwingman TA, Sunkin SM, Oh SW, Zariwala HA, Gu H, Ng LL, Palmiter RD, Hawrylycz MJ, Jones AR, et al. A robust and high-throughput Cre reporting and characterization system for the whole mouse brain. Nat Neurosci. 2010; 13:133–140. [PubMed: 20023653]

Merkle FT, Tramontin AD, García-Verdugo JM, Alvarez-Buylla A. Radial glia give rise to adult neural stem cells in the subventricular zone. Proc Natl Acad Sci U S A. 2004; 101:17528–17532. [PubMed: 15574494]

Merkle FT, Mirzadeh Z, Alvarez-Buylla A. Mosaic organization of neural stem cells in the adult brain. Science. 2007; 317:381–384. [PubMed: 17615304]

Ming GL, Song H. Adult neurogenesis in the mammalian brain: significant answers and significant questions. Neuron. 2011; 70:687–702. [PubMed: 21609825]

Mirzadeh Z, Merkle FT, Soriano-Navarro M, Garcia-Verdugo JM, Alvarez-Buylla A. Neural stem cells confer unique pinwheel architecture to the ventricular surface in neurogenic regions of the adult brain. Cell Stem Cell. 2008; 3:265–278. [PubMed: 18786414]

Miyata T, Kawaguchi A, Okano H, Ogawa M. Asymmetric inheritance of radial glial fibers by cortical neurons. Neuron. 2001; 31:727–741. [PubMed: 11567613]

Morrison SJ, Kimble J. Asymmetric and symmetric stem-cell divisions in development and cancer. Nature. 2006; 441:1068–1074. [PubMed: 16810241]

Morrison SJ, Hemmati HD, Wandycz AM, Weissman IL. The purification and characterization of fetal liver hematopoietic stem cells. Proc Natl Acad Sci U S A. 1995; 92:10302–10306. [PubMed: 7479772]

Noctor SC, Martínez-Cerdeño V, Ivic L, Kriegstein AR. Cortical neurons arise in symmetric and asymmetric division zones and migrate through specific phases. Nat Neurosci. 2004; 7:136–144. [PubMed: 14703572]

Paredes MF, Sorrells SF, Garcia-Verdugo JM, Alvarez-Buylla A. Brain size and limits to adult neurogenesis. J Comp Neurol. 2016; 524:646–664. [PubMed: 26417888]

Pastrana E, L-C C, Doetsch F. Simultaneous prospective purification of adult subventricular zone neural stem cells and their progeny. Proceedings of the National Academy of Sciences. 2009; 106:6387–6392.

Paton JA, O'Loughlin BE, Nottebohm F. Cells born in adult canary forebrain are local interneurons. J Neurosci. 1985; 5:3088–3093. [PubMed: 2414419]

Petreanu L, Alvarez-Buylla A. Maturation and death of adult-born olfactory bulb granule neurons: role of olfaction. J Neurosci. 2002; 22:6106–6113. [PubMed: 12122071]

Platel JC, Gordon V, Heintz T, Bordey A. GFAP-GFP neural progenitors are antigenically homogeneous and anchored in their enclosed mosaic niche. Glia. 2009; 57:66–78. [PubMed: 18661547]

Ponti G, Obernier K, Guinto C, Jose L, Bonfanti L, Alvarez-Buylla A. Cell cycle and lineage progression of neural progenitors in the ventricular-subventricular zones of adult mice. Proc Natl Acad Sci U S A. 2013; 110:E1045–E1054. [PubMed: 23431204]

Ramírez-Castillejo C, Sánchez-Sánchez F, Andreu-Agulló C, Ferrón SR, Aroca-Aguilar JD, Sánchez P, Mira H, Escribano J, Fariñas I. Pigment epithelium-derived factor is a niche signal for neural stem cell renewal. Nat Neurosci. 2006; 9:331–339. [PubMed: 16491078]

Reynolds BA, Weiss S. Generation of neurons and astrocytes from isolated cells of the adult mammalian central nervous system. Science. 1992; 255:1707–1710. [PubMed: 1553558]

Rompolas P, Mesa KR, Kawaguchi K, Park S, Gonzalez D, Brown S, Boucher J, Klein AM, Greco V. Spatiotemporal coordination of stem cell commitment during epidermal homeostasis. Science. 2016; 352:1471–1474. [PubMed: 27229141]

Sakaue-Sawano A, Kurokawa H, Morimura T, Hanyu A, Hama H, Osawa H, Kashiwagi S, Fukami K, Miyata T, Miyoshi H, et al. Visualizing Spatiotemporal Dynamics of Multicellular Cell-Cycle Progression. Cell. 2008; 132:487–498. [PubMed: 18267078]

Sanai N, Nguyen T, Ihrie RA, Mirzadeh Z, Tsai HH, Wong M, Gupta N, Berger MS, Huang E, Garcia-Verdugo JM, et al. Corridors of migrating neurons in the human brain and their decline during infancy. Nature. 2011; 478:382–386. [PubMed: 21964341]

Sawamoto K, Wichterle H, Gonzalez-Perez O, Cholfin JA, Yamada M, Spassky N, Murcia NS, Garcia-Verdugo JM, Marin O, Rubenstein JLR, et al. New neurons follow the flow of cerebrospinal fluid in the adult brain. Science. 2006; 311:629–632. [PubMed: 16410488]

Shahriyari L, Komarova NL. Symmetric vs. asymmetric stem cell divisions: an adaptation against cancer? PLoS One. 2013; 8:e76195. [PubMed: 24204602]

Shen Q, Goderie SK, Jin L, Karanth N, Sun Y, Abramova N, Vincent P, Pumiglia K, Temple S. Endothelial cells stimulate self-renewal and expand neurogenesis of neural stem cells. Science. 2004; 304:1338–1340. [PubMed: 15060285]

Shen Q, Qin S, Yue W, Erzsebet K, Gang L, Shu-Mien C, Goderie SK, Badrinath R, Sally T. Adult SVZ Stem Cells Lie in a Vascular Niche: A Quantitative Analysis of Niche Cell-Cell Interactions. Cell Stem Cell. 2008; 3:289–300. [PubMed: 18786416]

Shook BA, Manz DH, Peters JJ, Kang S, Conover JC. Spatiotemporal changes to the subventricular zone stem cell pool through aging. J Neurosci. 2012; 32:6947–6956. [PubMed: 22593063]

Snippert HJ, van der Flier LG, Sato T, van Es JH, van den Born M, Kroon-Veenboer C, Barker N, Klein AM, van Rheenen J, Simons BD, et al. Intestinal crypt homeostasis results from neutral competition between symmetrically dividing Lgr5 stem cells. Cell. 2010; 143:134–144. [PubMed: 20887898]

Spassky N, Merkle FT, Flames N, Tramontin AD, García-Verdugo JM, Alvarez-Buylla A. Adult ependymal cells are postmitotic and are derived from radial glial cells during embryogenesis. J Neurosci. 2005; 25:10–18. [PubMed: 15634762]

Tavazoie M, Masoud T, Van der Veken L, Violeta SV, Marjorie L, Lucrezia C, Bushra Z, Garcia-Verdugo JM, Fiona D. A Specialized Vascular Niche for Adult Neural Stem Cells. Cell Stem Cell. 2008; 3:279–288. [PubMed: 18786415]

Wang C, Liu F, Liu YY, Zhao CH, You Y, Wang L, Zhang J, Wei B, Ma T, Zhang Q, et al. Identification and characterization of neuroblasts in the subventricular zone and rostral migratory stream of the adult human brain. Cell Res. 2011; 21:1534–1550. [PubMed: 21577236]

Wichterle H, Garcia-Verdugo JM, Alvarez-Buylla A. Direct evidence for homotypic, glia-independent neuronal migration. Neuron. 1997; 18:779–791. [PubMed: 9182802]

Zappaterra MD, Lisgo SN, Lindsay S, Gygi SP, Walsh CA, Ballif BA. A comparative proteomic analysis of human and rat embryonic cerebrospinal fluid. J Proteome Res. 2007; 6:3537–3548. [PubMed: 17696520]

Zhuo L, Sun B, Zhang CL, Fine A, Chiu SY, Messing A. Live astrocytes visualized by green fluorescent protein in transgenic mice. Dev Biol. 1997; 187:36–42. [PubMed: 9224672]

Highlights

- V-SVZ neurogenesis is sustained by symmetric divisions of neural stem cells (NSCs)
- NSCs symmetrically self-renew and generate neurons later in life
- Symmetric consuming NSC divisions generate transient-amplifying cells
- With time, some self-renewed NSCs lose apical contact with the ventricle

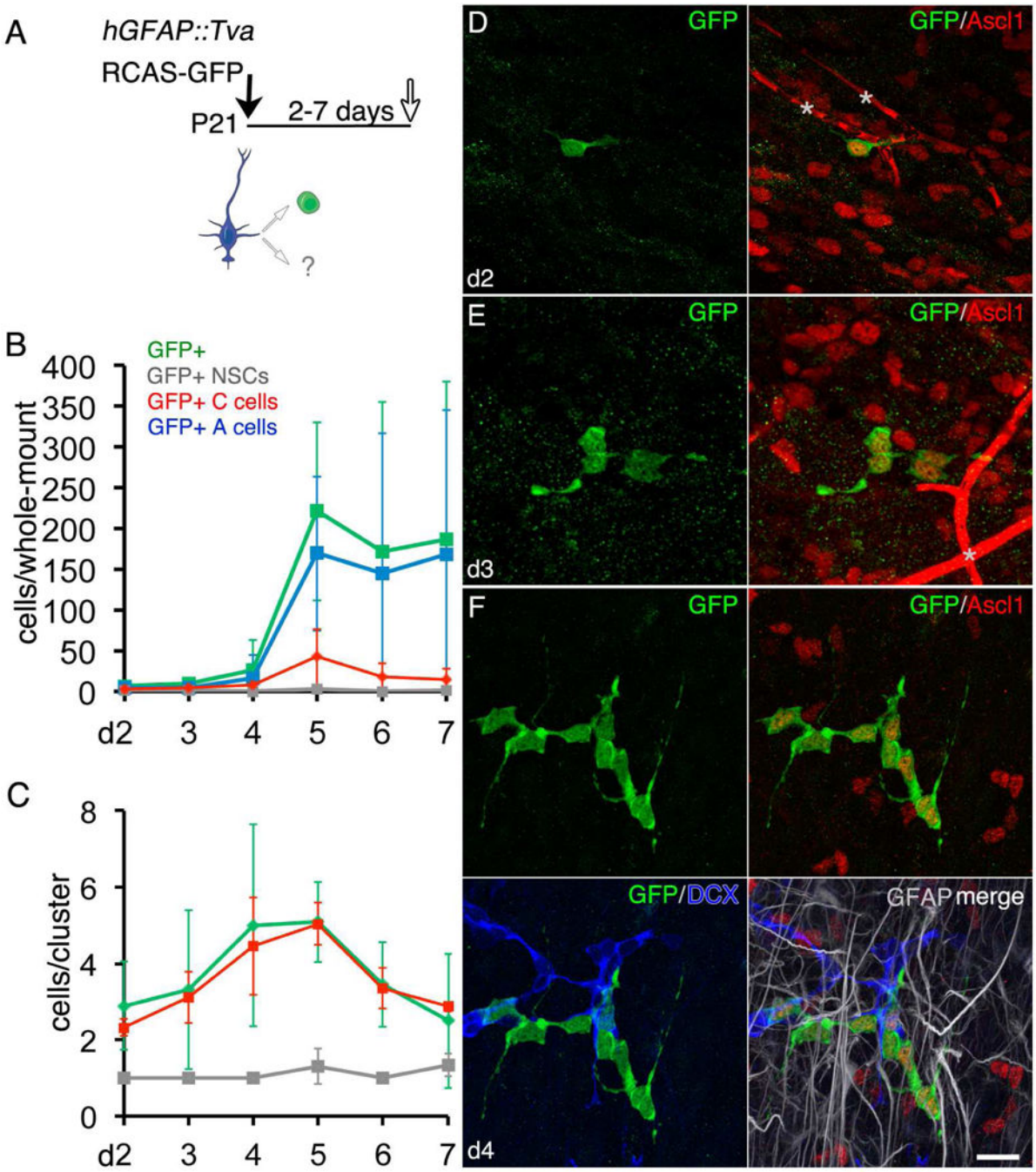

Figure 1. NSCs mostly generate C cells (see also Fig. S1 and Tabs. S1&S2)

(A) Experimental outline: Postnatal *hGFAP::Tva* mice received RCAS-GFP intraventricular, V-SVZ whole-mounts were prepared 2-7d later (note: only one of the two daughter cells upon division will carry the GFP label, see illustration). (B) After d4, the total number of GFP+ cells and GFP+ neuroblasts increases, the number of GFP+ C cells declines. (C) Cluster size increases until d4 (d2 vs. d4 $p= 0.0413$*; d2 vs. d5 $p < 0.0001$****), then declines (with; d3 vs. d5 $p= 0.054$*; d5 vs. d7 $p= 0.0116$*) (one-way ANOVA with Tukey's multiple comparisons). (D-F) GFP+ clusters grow in size from d2-d4; the majority express

Ascl1. Scale bar: 20 μm; asterisks indicate blood vessels revealed by antibodies raised in mouse (Ascl1) used on unperfused tissue (whole-mounts). Data in (B,C) are represented as mean +/− SD.

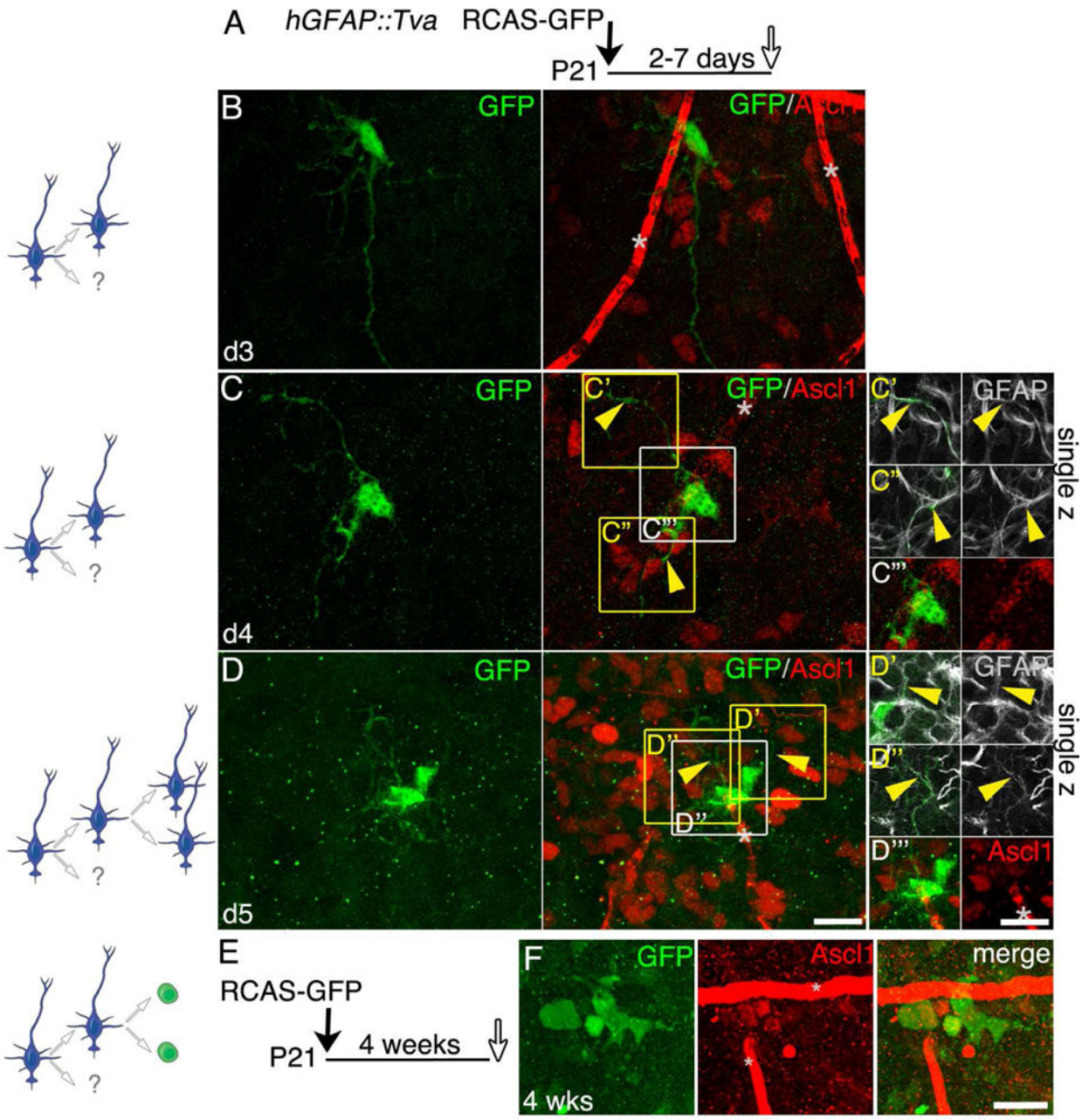

Figure 2. A subpopulation of NSCs self-renews (see also Tabs. S1&S2)

(A) Experimental outline for (B-D): Postnatal *hGFAP::Tva* mice received RCAS-GFP intraventricular, V-SVZ whole-mounts were prepared 2-7d later. (B-C) GFP+ secondary NSCs express GFAP (yellow arrowheads; C′-C″,D′-D″) and are Ascl1- (C‴, D‴). (D) A pair of (tertiary) GFAP+ NSCs on d5, suggesting a second self-renewing division. (E) Experimental outline for (F): Postnatal *hGFAP::Tva* mice received RCAS-GFP intraventricular, V-SVZ whole-mounts were prepared after 4 weeks. (F) A C cell cluster devoid of NSCs, indicating reactivation and consumption of a secondary NSC. Scale bars: 20 μm; asterisks indicate blood vessels revealed by antibodies raised in mouse (Ascl1) used on unperfused tissue.

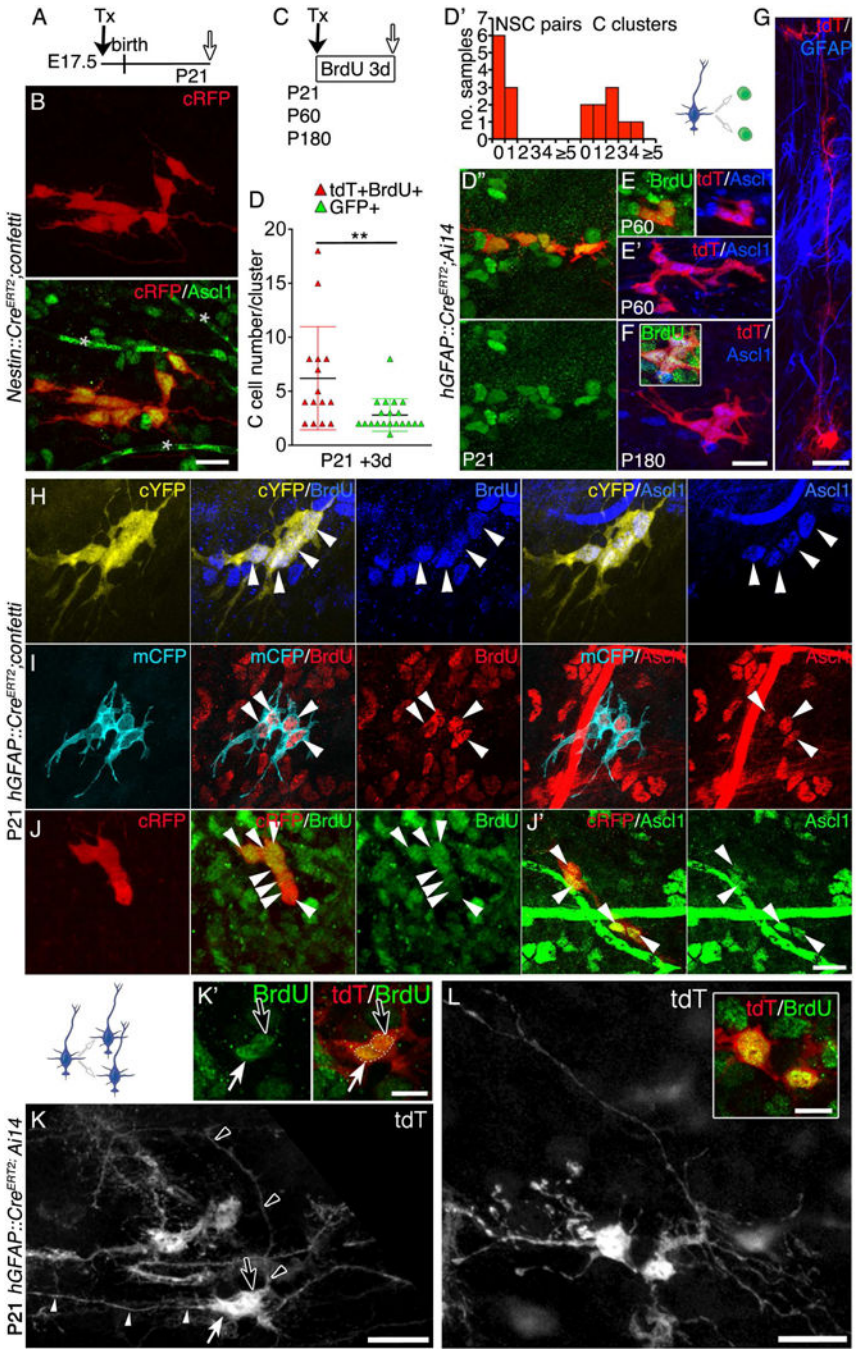

Figure 3. NSCs divide symmetrically (see also Fig. S2 and Tabs. S1, S3, S4)

(A) Experimental outline for (B): Time-mated pregnant *Nestin::Cre^{ERT2};confetti* mice received one low dose of Tx at E17.5, V-SVZ whole-mounts of the offspring were prepared at P21. (B) A cluster of cRFP+Ascl1+ C cells devoid of NSCs. (C) Experimental outline for (D-L): at P21 (D, H-L), P60 (E) or P180 (F) *hGFAP::Cre^{ERT2};Ai14* (D-G) or *hGFAP::Cre^{ERT2};confetti$^{+/WT}$* (H-J) mice received one injection of Tx and 3d of BrdU (drinking water). (D) On d3 clusters of tdT+BrdU+ cells are ~2-fold bigger than RCAS-GFP + clusters (p= 0.005**; two-tailed student's t-test with equal variance) (also see Fig. 1C). (D

′) Number of tdT+ events after cell division (tdT+BrdU+ NSC pairs or C cell clusters)/ whole-mount in *hGFAP::Cre^{ERT2};Ai14* mice after labeling at P21. (D″-F) Clusters of tdT +BrdU+ cells devoid of NSCs after labeling at P21 (D″), P60 (E), or P180 (F), indicating symmetric consuming divisions (differentiation). (G) A tdT+ GFAP+ NSC differs in morphology and cell size compared to C cells. (H-J) *hGFAP::Cre^{ERT2};confetti$^{+/WT}$* mice: clusters of C cells expressing cytoplasmic YFP (H) or RFP (J), or membrane-bound CFP (I), are Ascl1+BrdU+ and devoid of NSCs (YFP and CFP revealed by anti-GFP antibodies). (K-L) Pairs of tdT+BrdU+ NSCs in *hGFAP::Cre^{ERT2};Ai14* mice on d3, indicating symmetric self-renewal. Arrowheads in (K) denote the basal processes, arrows in (K′) the BrdU+ nucleus. Scale bars: 10 μm in (K′); all others 20 μm; asterisks indicate blood vessels revealed by antibodies raised in mouse used on unperfused tissue. Data in (D) are represented as mean +/− SD.

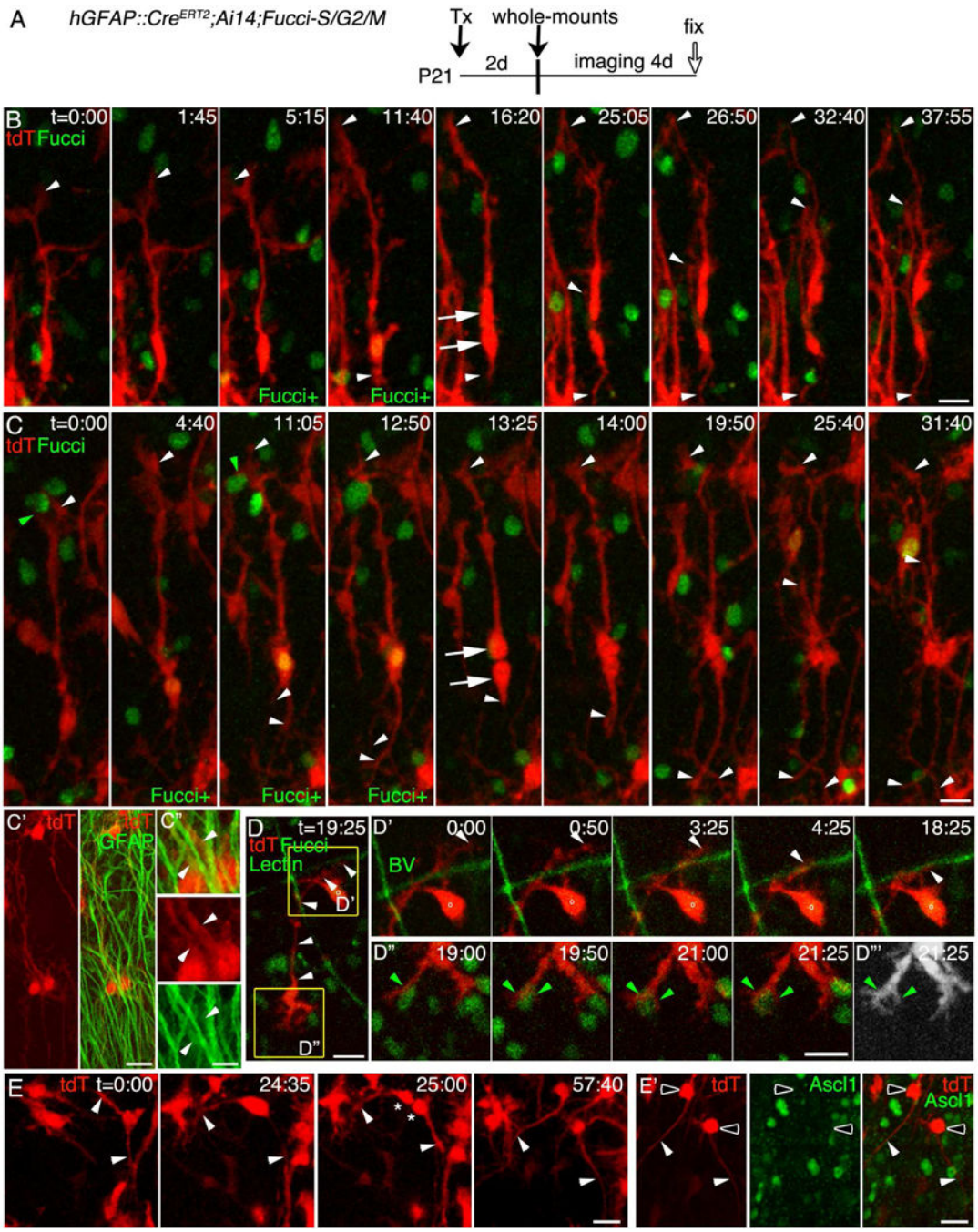

Figure 4. NSCs undergo symmetric self-renewing divisions *ex vivo* (see also Fig. S3 and movies S1&S2)

(A) Experimental outline: Postnatal *hGFAP::Cre^{ERT2};Ai14;FucciS/G2/M* mice received one injection of Tx, whole-mount explants were prepared on d2 and tissue was imaged up to 4 days before fixed for immunohistochemistry. (B) A tdT+ NSC with its basal process (white arrowhead at t=0:00 and throughout), becomes Fucci+ (azami-green+; t=11:40) while outgrowing a second, smaller process (white arrowhead). The basal process is maintained upon division (t=16:20), the daughter cell outgrowth a long process (white arrowhead) in parallel to the mother cells basal process (also see movie S1). (C) A tdT+ NSC with its basal

process (white arrowhead at t=0:00 and throughout), contacts other dividing (Fucci+) cells (green arrowhead in t=0:00), becomes Fucci+ (t=11:05) and outgrows two processes opposite of the basal process. After cell division (t=13:25; arrows) the mother cell maintains its basal process, the daughter cell outgrows a parallel process (t=25:40 and 31:40) (also see movie S1). Both cells are GFAP+ (C′&C″). (D) A NSC basal process shifts along blood vessels (BV; Lectin-Alexa488+; white arrowhead in D′), lateral processes contact and wrap around proliferating cells (green arrowhead in D″; gray scale image in D″; also see green arrowheads in C). (E) A dividing NSC harboring two long processes in opposite directions (white arrowheads in t=0:00) before division (t=25:00), generating two cells each inheriting one process. Both cells have NSC morphology and are Ascl1- (E′). Scale bars: 50 μm (B&C), 20 μm (C′, E&E″, D) and 10 μm (B′&C″). White arrowheads indicate basal processes; green arrowheads indicate contacts with proliferating (Fucci+) cells; o in (D) indicates a neighboring cell. Time (t) is in hh:mm. BV= blood vessel.

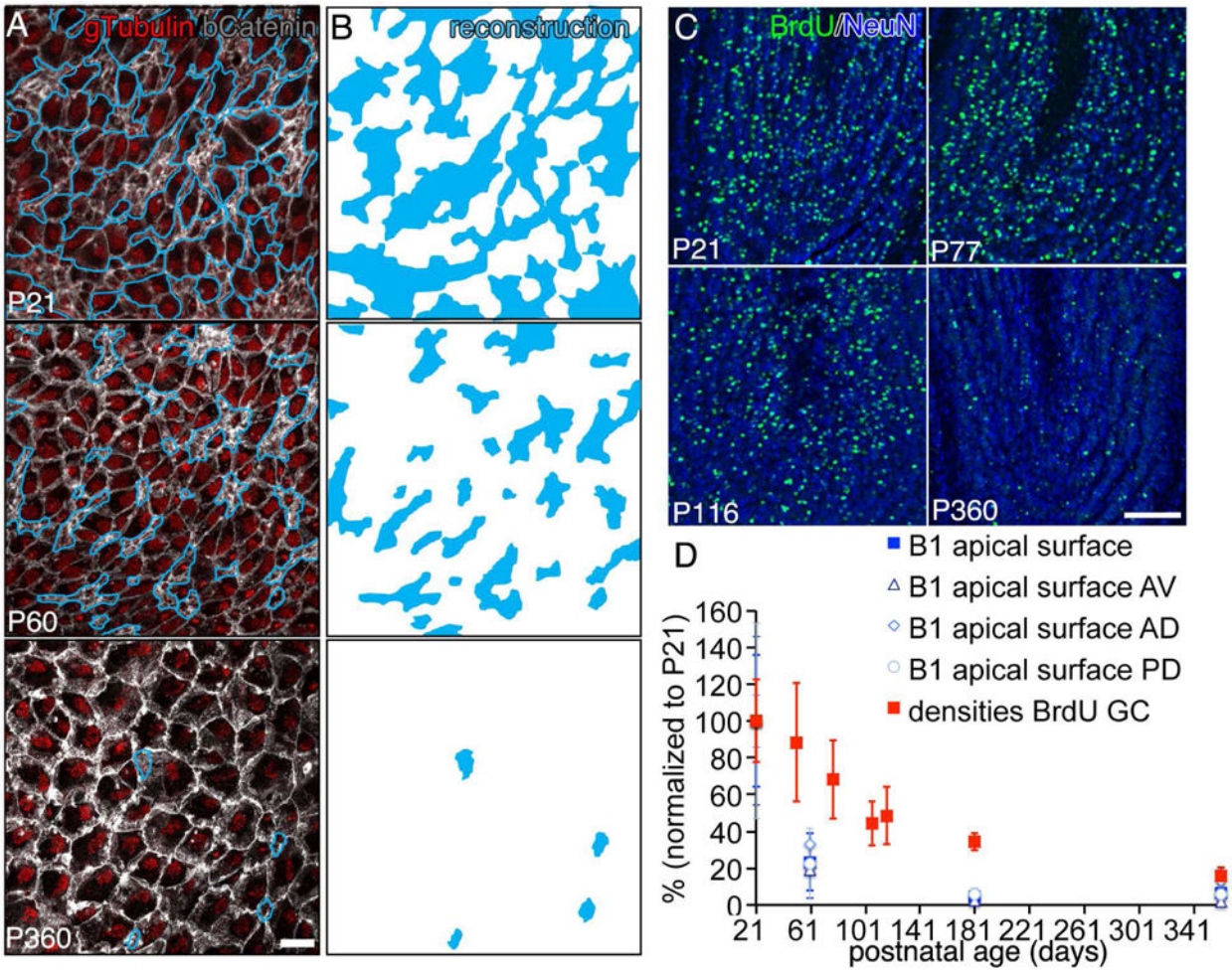

Figure 5. B1 cells and neurogenesis decline at different rates (see also Fig. S4)

(A,B) Apical contacts of B1 cells in the anterior-ventral (AV) lateral wall, revealed by beta-Catenin and gamma-Tubulin staining (A); pinwheel centers depicted in blue and in 2D tracings in (B). (C) Birth-dating of newborn (BrdU+) neurons (NeuN+) in the GC layer. Ages indicate time of BrdU administration. (D) Densities (cells/mm^2) of B1 cells apical contacts (blue symbols) in different regions of the V-SVZ and newborn granule neurons (red square) at different ages normalized to P21. X-axis indicates ages when apical contacts (B1 cells) were counted or BrdU was administered. Data are represented as mean +/− SD. Scale bar: 15 μm. GC granule cell.

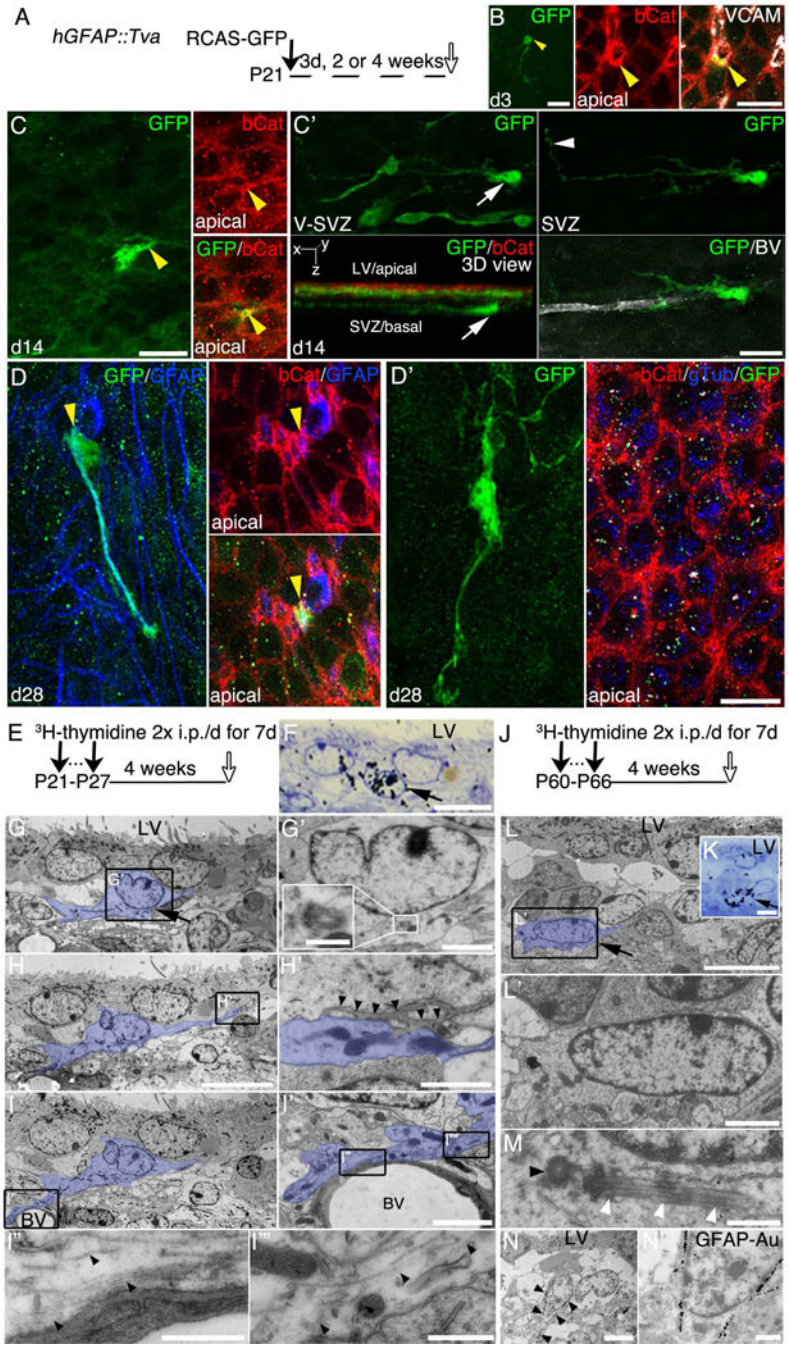

Fig. 6. A subpopulation of secondary NSC corresponds to non-apical B2 cells (also see to Fig. S5)

(A) Experimental outline for (B-D): Postnatal *hGFAP::Tva* mice received RCAS-GFP intraventricular, whole-mounts were prepared 3d, 2 weeks, or 4 weeks later. (B-D) Representative examples of secondary GFP+ cells at different time-points. (B) Secondary GFP+ B1 cells on d3 with apical contacts revealed by beta-Catenin and VCAM staining (yellow arrowheads). (C) Secondary GFP+ NSCs 2 weeks after injection with apical contact (B1 cells in C, yellow arrowheads) and without (in C′). Note: the non-apical GFP+ NSCs in C′ (white arrow) has typical NSC morphology (white arrowhead: long process; yellow

arrowhead: contact with BV) but is located beneath a layer of neuroblasts (see 3D image in second panel from top; apical surface revealed by beta-Catenin staining). (D) Secondary GFAP+GFP+ B1 cell 4 weeks after RCAS injection with apical contact (yellow arrowheads in D) or without (D′). (E) Experimental outline for (F-I): Postnatal *hGFAP::GFP* mice received two i.p. injections of ^{3}H-thymidine/day for 7d. Semithin (autoradiography) or ultrathin (TEM) coronal sections were analyzed after 4 weeks. (F) Autoradiography of toluidine blue-stained semithin section of the V-SVZ showing a ^{3}H-thymidine+ LRC (arrow). (G-I) Pseudo-colored serial TEM micrographs of the LRC shown in (F), characterized as B2 cell. The primary cilium is located at the basal side (not towards the LV; tangential section of the cilium in insert in G′), cytoplasmic expansions contact extracellular matrix (fractones; H and arrowheads in H′) and the basal lamina of a blood vessel (I, I′); intermediate filaments are shown in (I″, I‴). (J) Experimental outline for (K-N): Adult (P60) *hGFAP::GFP* mice received two i.p. injections of ^{3}H-thymidine/day for 7d. Semithin (autoradiography) or ultrathin (TEM) coronal sections were analyzed after 4 weeks. (K) Autoradiography of a toluidine blue-stained semithin section of the V-SVZ showing a ^{3}H-thymidine+ LRCs (arrow). (L) Pseudo-colored TEM micrograph of the LRC shown in (K), characterized as B2 cell with typical astrocytic ultrastructure (L′). The 9+0 primary cilium (white arrowheads) and its daughter centriole (black arrowhead) of the LRC is at the basal side (not towards the LV) (M). (N) A GFAP immunogold (arrowheads) labeled B2 cell showing an expansion through the parenchyma. Scale bars: 20 μm (B-D); 10 μm (F-H, K), 5 μm (L, N), 2 μm (G′, I′, L′), 1 μm (H′, N′), 500 nm (G″, I″, I‴, M).

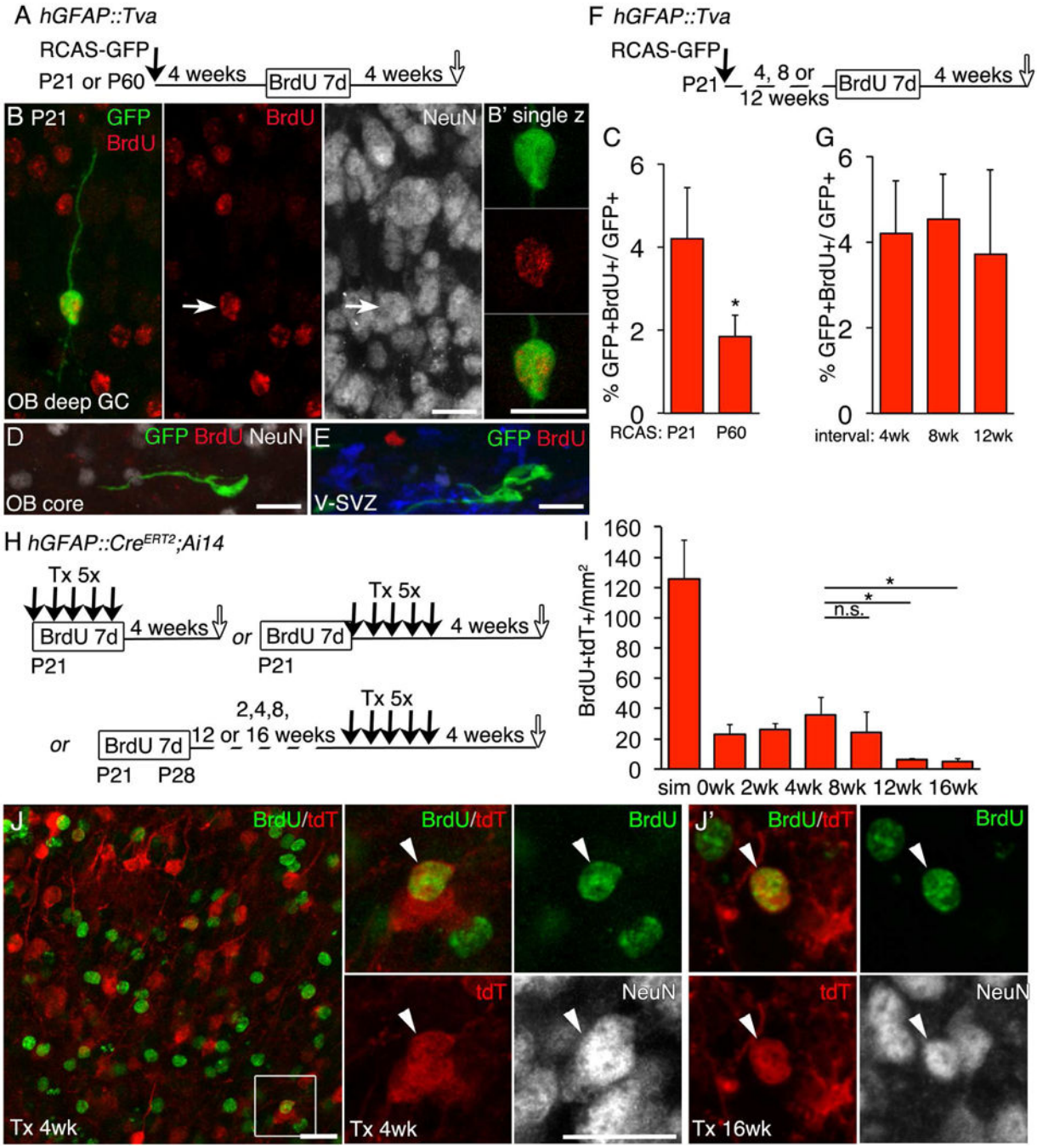

Figure 7. Self-renewing NSCs generate OB interneurons later in life (see also Fig. S6 and Tabs. S5&S6)

(A) Experimental outline for (B-E): Postnatal (P21) or adult (P60) *hGFAP::Tva* mice received RCAS-GFP intraventricular and BrdU (1 week drinking water) 4 weeks later. Forebrain and OB were analyzed in coronal sections after 4 additional weeks. (B) A GFP +BrdU+ granule neuron upon viral injection at P21. (C) Percentages of GFP+BrdU+ OB interneurons born 4 weeks after viral injection (p= 0.021*; two-tailed student's t-test with equal variance). (D,E) GFP+ neuroblasts in the core of the OB (D) and V-SVZ (E) upon viral injection at P21. (F) Experimental outline for (G): Postnatal *hGFAP::Tva* mice received

RCAS-GFP intraventricular and BrdU (1 week drinking water) 4, 8, or 12 weeks later. Forebrain and OB were analyzed in coronal sections after 4 weeks. (G) Percentages of GFP +BrdU+ OB interneurons born 4, 8, or 12 weeks after viral injection at P21. (H) Experimental outline for (I,J): Postnatal *hGFAP::Cre^{ERT2}:Ai14* mice received BrdU (drinking water) for 1 week (P21-P28) and one daily injection of Tx for 5 days at different ages: i) simultaneously with BrdU at P21 (sim), ii) directly after BrdU treatment at P28 (0wk), or iii) 2, 4, 8, 12 or 16 weeks after BrdU treatment. Coronal sections of the OB were prepared 4 weeks after the last Tx injection. (I) Density of BrdU+tdT+ interneurons (4wk vs. 8wk, p= 0.22, n.s.; 4wk vs. 12 wk, p= 0.022 *; 4wk vs 16 wk, p= 0.05 *; student's t-test with equal variance). X-axis indicates interval between BrdU and Tx. (J) BrdU+tdT+NeuN+ interneurons born at least 4 weeks or 16 weeks (J′) after BrdU administration. Note that these cells are brightly labeled with BrdU. Data are represented in (C, G, I) as mean +/− SD. Scale bars: 20 μm (J); 15 m; (B, D); white arrows in (B) indicate GFP+BrdU+NeuN+ interneurons; white arrowheads in J indicate BrdU+tdT+NeuN+ interneurons; GC granule cell.